ENVIRONMENTAL MONITORING

using Diode-Laser-Based Spectroscopic Techniques

Gabriel Somesfalean

Doctoral Thesis
Department of Physics
Lund Institute of Technology

November 2004

Printed in Sweden by KFS AB, Lund, 2004

Department of Physics
Lund Institute of Technology
P. O. Box 118
SE-221 00 Lund
SWEDEN

Lund Reports on Atomic Physics, LRAP-329

ISSN 0281-2762

ISBN 91-628-6286-3

To my Family,
for a more Human World

CONTENTS

ABSTRACT

Monitoring of environmental gases is necessary to understand the complex processes governing global warming and the impact of pollutant emissions related to human activity. Diode-laser-based spectroscopic techniques, being robust and affordable, have a great potential to become an industrially well-established technology for environmental sensing. This thesis deals with the further development of these techniques, demonstrated in several applications to atmospheric gas detection and sensing.

The accessible spectral range of tunable diode lasers was extended by use of sum-frequency generation. High-resolution ultraviolet spectroscopy of mercury isotopes around 254 nm was performed on low-pressure cells as well as at atmospheric pressure. Ultraviolet radiation around 300 nm, utilized for monitoring of sulfur dioxide and studies of the pressure dependence of the absorption spectrum, was produced using a sum-frequency generation scheme employing a blue and a near-infrared diode laser.

Detection sensitivity was improved by several orders of magnitude by employing frequency modulation techniques. This was demonstrated with blue continuous-wave diode lasers in measurements on ground state potassium atoms, and lead atoms in very weakly populated meta-stable states. In the red spectral region, traffic-generated emission of nitrogen dioxide was monitored *in situ* using long path absorption at a wavelength around 635 nm.

A new temporal gas-correlation scheme was developed, which overcomes the intrinsic multimode and mode-jump behaviour of diode lasers. The concentration of a gas under study is determined by temperature tuning the wavelength of a diode laser across an absorption band of the gas, and by simultaneous temporal correlation of the detected signal with the signal from a known reference gas concentration. No knowledge of the exact spectrum is needed. The method was tested in diffusion related measurements.

A novel technique for analysis of free **ga**s in **s**cattering **m**edia by use of **a**bsorption **s**pectroscopy, GASMAS, was introduced. The sharp absorption features of the gas, contrasted to the very slow wavelength dependence of the bulk material, can be picked up by use of modulation techniques. Dispersed molecular oxygen embedded in various natural and man-made porous materials was detected and measured. The gas concentration was determined by combining absorption and time-resolved laser spectroscopy measurements. Investigations were performed to assess the internal gas pressure and gas diffusion characteristics.

A new single-aerosol particle detector using a coupled-cavity diode laser was developed. Simultaneous size and shape determination was demonstrated by recording of the optical extinction and a diffraction image in the near-forward scattered light.

LIST OF PUBLICATIONS

This thesis is based on the following papers, which will be referred to by their Roman numerals in the text.

Paper I U. Gustafsson, G. Somesfalean, J. Alnis, and S. Svanberg, *Frequency modulation spectroscopy with blue diode lasers*, Applied Optics **39**, 3774-3780 (2000).

Paper II G. Somesfalean, J. Alnis, U. Gustafsson, H. Edner, and S. Svanberg, *Long-path monitoring of NO_2 with a 635 nm diode laser using frequency modulation spectroscopy*, submitted 2004.

Paper III J. Alnis, U. Gustafsson, G. Somesfalean, and S. Svanberg, *Sum-frequency generation with a blue diode laser for mercury spectroscopy at 254 nm*, Applied Physics Letters **76**, 1234-1236 (2000).

Paper IV G. Somesfalean, Z.G. Zhang, M. Sjöholm, and S. Svanberg, *All-diode-laser ultraviolet absorption spectroscopy for sulfur dioxide detection*, submitted 2004.

Paper V J. Sandsten, U. Gustafsson, and G. Somesfalean, *Single aerosol particle sizing and identification using a coupled-cavity diode laser*, Optics Communications **168**, 17-24 (1999).

Paper VI M. Sjöholm, G. Somesfalean, J. Alnis, S. Andersson-Engels, and S. Svanberg, *Analysis of gas dispersed in scattering media*, Optics Letters **26**, 16-18 (2001).

Paper VII G. Somesfalean, M. Sjöholm, J. Alnis, C. af Klinteberg, S. Andersson-Engels, and S. Svanberg, *Concentration measurement of gas embedded in scattering media by employing absorption and time-resolved laser spectroscopy*, Applied Optics **41**, 3538-3544 (2002).

Paper VIII J. Alnis, B. Andersson, M. Sjöholm, G. Somesfalean, and S. Svanberg, *Laser spectroscopy on free molecular oxygen dispersed in wood materials*, Applied Physics B **77**, 691-695 (2003).

Paper IX G. Somesfalean, M. Sjöholm, L. Persson, H. Gao, T. Svensson, and S. Svanberg, *Spectroscopic gas analysis using a new temporal gas correlation technique*, submitted 2004.

Additional material has been presented in the following scientific papers:

G. Somesfalean, J. Alnis, S. Svanberg, A. Derkatch, S. Mannervik, D. Rostohar, P. Royen, P. Schef, L.-O. Norlin, *Violet diode lasers in time-resolved stored-ion spectroscopy*, Physica Scripta **69**, 98-103 (2004).

E. Biémont, P. Palmeri, P. Quinet, G. Paquin, Z.G. Zhang, G. Somesfalean, S. Svanberg, *Measurement of radiative lifetimes and determination of transition probabilities of astrophysical interest in Ho III*, Monthly Notices of the Royal Astronomical Society **328**, 1085-1090 (2001).

Z.G. Zhang, G. Somesfalean, S. Svanberg, P. Palmeri, P. Quinet, E. Biémont, *Radiative lifetime measurements and oscillator strengths of astrophysical interest in Ho III*, Astronomy & Astrophysics **384**, 364-370 (2002).

J. Nordqvist and G. Somesfalean, *Why industries environmental performance doesn't count*, China Environment Series **6**, 136-139 (2003).

J. Nordqvist and G. Somesfalean, *Perspectives on performance and policy in industry – environmental and quality concerns to enhance energy efficiency*, ECEEE 2003 Summer Study – Time to Turn Down Energy Demand, 783-790 (2003).

PART I

CHAPTER 1

INTRODUCTION

> We call it *ljus*, *light*, 光, *fény*, *Licht*, *lumière, Prakash, luce, ukukhanya, luz, nour, gaisma, Roshni, CBET, …*

Light has always had an almost magical meaning for us. We perceive the reality around us through our senses, maybe to the largest extent through our sight. Human vision, based on light reflection and pattern recognition, mostly focuses on structural features and conveys to us information about shapes, color, distance, movement, etc. However, light has also helped us to elucidate the world under the microscope or to scan the depths of space in astronomy. Optics, the study of light, can perhaps be dated back to the first use of the lens by Aristophanes about 423 B.C. In more recent years, by decomposing light in its wavelength components, spectroscopy has taught us most of what we know about the physics of matter and light.

Because of the wavelength-specific interplay between electromagnetic radiation and matter it is possible to gain information about the microcosmos, such as atoms and molecules in the environment. Each atom or molecule is uniquely characterized by a set of energy levels. Resonant transitions between different levels by absorption or emission of electromagnetic radiation result in highly specific spectroscopic features. These spectroscopic "fingerprints" allow both the identification and quantification of the particular species, such as atmospheric gases. Even if the incoming electromagnetic radiation is not resonant with the energy separation in an atom or molecule, a weaker type of interaction process can occur, namely that of scattering. Scattering phenomena are extremely common in nature. Light propagating through the atmosphere is scattered by molecules and aerosol particles, a process responsible for the blue of the clear sky and the red of the setting sun. The basic light-matter interactions that occur in atoms and molecules are shown schematically in Fig. 1.1.

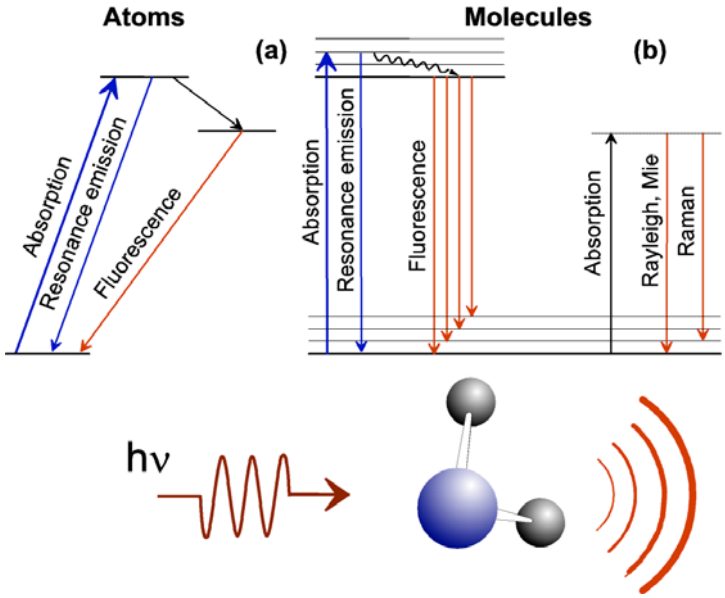

Fig. 1.1 *Schematic illustration of the light-matter interaction processes in atoms and molecules: (a) resonant transitions (b) non-resonant scattering processes.*

The atmosphere – being a multi-layered, mainly transparent body surrounding the Earth – can easily by studied using light. The atmosphere consists of a complex and dynamic mixture of gases, vapor, and aerosol particles. The major constituent, disregarding nitrogen, is the oxygen we breathe. Plants produce this life-essential gas through photosynthesis, a process inherited from its "inventor", the ancient cyanobacteria [1]. The atmosphere also contains numerous trace gases whose sources are both natural and anthropogenic. The trace gases play a key role in atmospheric chemistry processes and have large implications on the environmental condition on our planet. Gases can also be found in porous media, e.g., encapsulated in porous plants and stone, foodstuff we eat, synthetic materials (such as catalysts for automobile exhaust), gas bubbles in ice cores (containing traces of the ancient atmospheric composition), etc. The composition of the atmosphere is constantly changing, but there is no doubt that this process has recently been accelerating because of human activities.

It has been recognized that the main source of global climate change is human-induced changes in atmospheric composition [2]. These perturbations primarily result from emissions associated with an increased energy use, a result of the growth of the world's human population and of anthropogenic activities. Tropospheric air pollution has impacts on scales ranging from local to global. Industrial air pollution from fossil fuel combustion as well as emissions from biomass burning – such as forest fires and agricultural waste burning – can affect air quality where people live and work. Outlets to the atmosphere have resulted in environmental alarms such as global warming,

depletion of the stratospheric ozone layer, and serious urban pollution. Serious damage from acid precipitation caused by emissions of sulfur dioxide already afflicts vast regions of the industrialised and developing countries. The global aspects of pollution have been revealed in observations of various tropospheric air pollutants such as NO_2, SO_2, and HCHO made by the Global Ozone Monitoring Experiment (GOME) and the Scanning Imaging Absorption Spectro-Meter for Atmospheric CartographY (SCHIAMACHY) satellites [3].

One of the greatest challenges humanity is facing today is to understand the complex issue of environmental change. The awareness of the environmental problems caused by both anthropogenic and natural emissions has increased during the last decades. Demands are being raised for more efficient and cleaner production methods in industry and reduced pollutant emission from, e.g., automobile traffic and heating devices. Environmental monitoring provides very important means, which can help us in the protection of our environment and to fight against pollution.

The work presented in this thesis aims at developing advanced spectroscopic techniques that can be used for environmental sensing. The main emphasis is on the employment of tunable diode laser spectroscopy in the development of various gas and aerosol-particle sensors. Most of the work presented involves aspects of absorption spectroscopy and light scattering.

With the advent of the laser in the previous century – especially tunable laser sources – a powerful tool has been made available to be utilized for basic research and for real-world applications. Owing to the narrow spectral bandwidth, high irradiance, and directionality of the laser radiation, laser-based spectroscopic techniques have rapidly been applied for sensitive and selective detection of various gaseous species. The laser type that has found the most widespread application, also (or mainly) outside the scientific laboratories, is the diode laser. Today, we find the diode lasers in our everyday life in applications ranging from telecommunications, compact disc players, optical memories, laser printers, bar-code readers to industrial process control and medical diagnostics. Diode laser spectrometers are now at the threshold of routine application in environmental monitoring for high-resolution trace gas detection and in the study of combustion processes. Clearly, diode lasers are particularly well suited for applications because of their realistic cost and convenience of operation.

Organization of the thesis

The thesis is divided into two parts, the first introductory part gives a background to the field of environmental monitoring and describes some of the techniques used in the present work, and the second part consists of the original scientific papers which are the basis of this thesis.

In Chapter 2 a brief presentation is given for some pollutant gases and aerosols of relevance for the work performed, together with a short review of currently used monitoring techniques. A brief discussion about requirements and possibilities for

deployment of environmental monitoring technology concludes this chapter. Tunable diode lasers and their characteristics for spectroscopic application are the topic of Chapter 3. In Chapter 4 important absorption relations are presented, together with a reference to available spectroscopic databases for atoms and molecules. Practical aspects of diode laser spectroscopy are further outlined. In Chapter 5 methods for achieving high sensitivity in absorption measurements are discussed and different sources of noise are presented. Chapter 6 discusses light scattering applications and includes a brief description of the theories used, as well as a presentation of a new technique for monitoring gases in porous materials. Chapter 7 describes the gas correlation technique and discusses its application in conjunction with diode lasers.

Two appendices are included in this thesis and they describe the coupled-cavity model used in Paper V, and the diffusion approximation theory discussed in Chapter 6, respectively.

CHAPTER 2

ENVIRONMENTAL MONITORING

Environmental pollution and climate change are truly global issues, which may prove to be humanity's greatest challenges. These two issues are very unlikely to be adequately addressed without greatly improved international co-operation and action. Effective pollution abatement strategies must be based on a detailed understanding of the causes and the effects of pollution. The analysis must be done on spatial scales ranging from local to regional and eventually to global. A wide range of techniques can be employed in enevironmental monitoring of tropospheric trace gases in ways that are appropriate to the different spatial scales.

Environmental monitoring comprises the atmosphere, the hydrosphere as well as land. In this work only the study of the atmosphere and some of its constituents is considered. Except for being motivated from needs to assess the influence of pollutants and control the efficiency of legislative actions, reliable detection of trace gases plays a crucial role in many real-world applications, including industrial emissions control (e.g., fence line perimeter monitoring in the petrochemical industry, combustion sites, waste incinerators, gas-pipe and compressor station safety), rural emissions control (e.g., horticultural greenhouses, fruit storage and rice agro-ecosystems), air quality monitoring (e.g., automobile traffic), chemical analysis and control for manufacturing processes (e.g., in the semiconductor, pharmaceutical, and food industries), medical and combustion diagnostics, detection of toxic gases, drugs, and explosives relevant to law enforcement and public safety.

Effective environmental management can only be achieved when a whole chain of actions are taken:

(1) starting from basic research and fundamental studies, where more knowledge is gained

(2) proceeding with industrial implementation that demonstrate the efficiency of the techniques

(3) finalizing with the decision-making and legislative processes, where suitable policies are designed and implementation of the regulations is ensured.

These three steps, if properly implemented, can make a large impact on the quality of life and ensure sustainable development.

2.1 Particles and Trace Gases in the Atmosphere

The atmosphere is a global commons that responds to many types of emissions into it. Global changes in atmospheric composition occur from anthropogenic emissions of greenhouse gases – that result mainly from the burning of fossil fuels – and methane and nitrous oxide from multiple human activities. Because these gases have long (decades to centuries) atmospheric lifetimes, the result is an accumulation in the atmosphere and a build-up in concentrations that are clearly shown by instrumental observations of air samples and in bubbles of air trapped in ice cores. Atmospheric air pollution has a long history [4]. From at least the 13th century up to the mid-20th century, documented air pollution problems were primarily associated with high concentrations of sulfur dioxide (SO_2) and soot particles. These problems are often dubbed "London Smog" because of a severe episode in that city in 1952.

The atmosphere contains thousands of trace gases, which affect atmospheric chemistry and human beings in one way or the other. Modern atmospheric chemistry is the study of trace gases, such as oxidants (O_3, OH, H_2O_2, HCHO, HO_2, and NO_3), gases that can be oxidized (hydrocarbons and sulfur compounds), oxidation products (carbonyls and organic nitrates), and the interaction of all these with aerosols and clouds. Below, a brief description is given of aerosol particles and a few important trace gases, which have connections to the work presented in the thesis.

Aerosol particles

The term *aerosol* (also called *particulate matter*) refers to an assembly of liquid or solid particles suspended in a gaseous medium. Natural processes generating aerosol particles include volcanic eruptions, sea spray and forest fires, as well as biological particles such as fungal spores, pollens, and viruses. Anthropegenic aerosol emissions originate mainly from combustion (e.g. automobile exhaust fumes, agricultural burning, tobacco smoke) and industrial processes. In the indoor environment, walls, floors, and ceilings may release fibres of hazardous materials. Aerosol particles may have a great diversity in size, shape, density, and chemical composition. The range of particle sizes extends over five decades from about 0.001 μm to about 100 μm. Particle size is the most important factor affecting transportation and deposition of aerosols. Especially particulate matter less than 10 μm in diameter, known as PM_{10}, has come under detailed scrutiny because it can reach the thoracic region and cause serious diseases. Most real aerosol systems consist of particles of irregular shape [5]. Characterization of airborne particles is critical in a wide range of fields, including industrial emissions and ambient air quality monitoring, as well as research on cloud

condensation with implications to earth radiation balance and global climate [6]. Health concerns have often driven the technology for detecting and quantifying airborne particles, since allergy, asthma and lung cancer are known to increase because of poor indoor air quality and high levels of particulate contaminants and pollen in the outdoor environment [7].

Sulfur dioxide, SO_2

Sulfur dioxide (SO_2) is both a natural pollutant and an anthropogenic product. It occurs in nature in volcanic smoke and gases. For example, fluxes of the order of 1000 tons/day have been measured for Mount Etna in Italy in non-eruptive conditions [8]. A wide rate of atmospheric sulfur dioxide is produced near industrial plants. Oil, coal and natural gas often contain sulfur compounds; thus, after combustion, SO_2 is widely present in gases released. Sulfur dioxide has a high toxicity. It easily dissolves in atmospheric water and produces sulfuric acid, which contributes to the acidification of water and soil (acid rain). It is also believed that sulfur dioxide emitted from volcanoes is converted to sulfate aerosols, which stay at high altitudes in the upper part of the troposphere and affect directly and indirectly the incoming solar radiation.

Nitrogen dioxide, NO_2

Nitrogen dioxide (NO_2) is the only pollutant gas that has a color. It appears as a reddish brown gas, because it absorbs visible light in the blue region of the spectrum. Although some NO_2 is emitted directly into the atmosphere by combustion processes, most of it is formed by the oxidation of nitrogen oxide, NO (the major nitrogenous by-product of combustion) after dilution in air. This conversion of NO to NO_2 occurs as part of the oxidation of organic compounds, initiated by reactive species such as the OH radical [9]. The oxides of nitrogen, NO_x ($NO_x \equiv NO + NO_2$) are produced by industrial combustion processes, automobile traffic, biomass burning and by lightning [10]. Anthropogenic NO_x emissions are now estimated to be 3-4 times the natural emissions, and they are expected to double again by 2020 [11]. Changes to NO_x have affected, and will continue to affect, atmospheric chemistry and composition on local, regional, and global scales. In urban areas, NO_x mixing ratios of 10-100 parts per billion are typical, while in the remote environments, concentrations of a few parts per trillion have been measured [12].

The oxides of nitrogen play a vital role in atmospheric chemistry despite their relative low abundance. They regulate production rates of ozone and OH in the troposphere [13], and destruction rates of ozone in the stratosphere [14]. It has also been shown that NO_x affects plant and animal life. The oxides of nitrogen are also precursors to nitrous acid, which contributes to acid precipitation and ecosystem

damage, particularly where soils are lacking sufficient alkalinity to buffer the acid. At high concentrations, especially prevalent in urban areas, NO_x is a toxic pollutant.

Heavy metals

Recent reports on metal species in the atmosphere have predicted significant increases of emissions from utilities firing solid fuels – especially coal, biomass and waste materials – and these contribute to the pressure on the environment [15]. Heavy metals of particular concern to public health include mercury (Hg), lead (Pb), cadmium (Cd), and arsenic (As), which are highly toxic and have relatively high vapor pressures.

Levels of trace metals found in air, food, water and soil/dust vary widely throughout the world and depend on factors such as industrial development, urbanisation and lifestyle. For example, ambient air levels of lead over 10 $\mu g/m^3$ have been reported in urban areas near smelters, whereas in cities where leaded petrol is no longer used, quantities of lead below 0.1 $\mu g/m^3$ have been found. In cities of developing countries, traffic-related lead levels range from 0.3-1 $\mu g/m^3$ with extreme annual mean values between 1.5 and 2 $\mu g/m^3$ [16]. Lead and other trace metals can be inhaled as fine particles and deposited in the lungs. Especially the small-mode (2.5 μm) particles are considered dangerous since they are inhaled much more deeply than the coarser particles. Hence, cost-effective methods for removing such species are required, and with them, sensitive, real-time process monitoring.

Mercury is the only trace gas that is primarily present in atomic form in the troposphere. Geophysical trace emissions of Hg originate from volcanoes, geothermal fields, mines and deposits. Mercury has long been used for many applications in industry, ranging from chlor-alkali plants, paper and pulp mills, to electronics, dentistry and disinfectants. The anthropogenic emission of Hg is ~3.5 Mkg/year, while natural sources and biogenic evaporation from the earth surface stand for ~2.5 Mkg/year [17]. For example, the Hg emission from chlor-alkali industry in Europe constitutes 14% of the total anthropogenic mercury emission [18]. Typical background concentrations of mercury in air are a few ng/m^3 [19], but much higher mercury concentrations exist around mercury mining areas and chlor-alkali plants [20]. Owing to the neurotoxic effects of mercury, increasing demands are put on industry and utilities to reduce emissions to the atmosphere. Measures to control releases to air and water have been implemented in many countries. Recently, an international agreement on emission controls of mercury has been signed by 32 countries from Europe, USA and Canada, within the framework of the LRTAP convention of the UN-ECE [21].

Table 1.1 *Limit values in the European Union of some important gases, aerosols, and metal vapors in the atmosphere.*

	SO_2 ($\mu g/m^3$)	NO_2 ($\mu g/m^3$)	PM_{10} ($\mu g/m^3$)	Pb ($\mu g/m^3$)
Hourly limit value for the protection of human health	350	200	-	-
Daily limit value for the protection of human health	125	-	50	-
Annual limit value for the protection of human health	-	40	40	0.5
Annual limit value for the protection of ecosystems	20	30	-	-

As a matter of reference, the allowed limit values for sulfur dioxide, nitrogen dioxide, particulate mater (PM_{10}), and lead in ambient air, according to the European Union Council directive, are listed in Table 1.1 [22].

2.2 Monitoring Techniques

There is an increased need to understand the processes involved in the enormous growth of anthropogenic trace gas emissions. Consequently, there is also considerable interest in techniques capable of monitoring these emissions, in order to find the best means to abatement and to ensure compliance with environmental legislation. A broad review of different spectroscopic techniques used for trace gas monitoring is presented in Ref. [23]. In this section only a brief survey of the monitoring techniques in use is presented.

Qualitative and quantitative analysis of trace gases and aerosol particles can be performed using both optical and non-optical techniques. The current instrumentation for gas analysis is characterized by a variety of different technologies, which are applied to different gases. This variety makes system integration difficult, requires many different calibration procedures and increases system costs. Some of these standard methods have slow response, low sensitivity and complicated preconcentration procedures.

The traditional approach to measure aerosols is to sample the particles onto a filter. This extractive method generally relies on experts to examine the filters under the microscope in a laboratory, which is a time-consuming procedure that usually cannot be carried out on site.

Many chemical sensors are used to measure tropospheric trace gases that cannot be measured by spectroscopic techniques. Chromatographs separate trace gases in a capillary, after which the gases are detected in a variety of ways. When the chromatograph is followed by a mass spectrometer, it provides unique fingerprints of the separated products. Sometimes the mass spectrometers are combined with chemical ionization. Sulfur dioxide measurements are frequently based upon ultraviolet (UV) fluorometric techniques or chemiluminescence, while mercury detection utilizes the gold amalgamation principle during accumulative sampling cycles. Currently, the predominant method of measuring concentrations of NO_2 involves reducing it to NO using a heated molybdenum catalyst, followed by detecting the chemiluminescent reaction of NO with ozone (O_3) [24]. This technique can reach a sensitivity in the parts-per-billion range, but its use entails a relatively complex and expensive apparatus. Other measurement techniques for NO_2 include chemiluminescence detection using luminol [25], and use of electrochemical cells [26].

Since 1926, when the first pioneering experiments were performed [27], spectroscopic techniques have become an increasingly important branch in atmospheric trace-gas monitoring. The main features of optical and spectroscopic techniques are the non-intrusive *in situ* detection capability, the possibility of remote sampling and easy coverage of large areas, high sensitivity and selectivity, as well as fast time response.

Optical registration methods are called passive if the sun or the thermal background radiation is utilized. An everyday usage of the passive techniques is visible (outdoor) light photography. Fourier transform infrared spectroscopy (FTIR) is one of the most common passive remote sensing technologies, and it is ideally suited for multicomponent analysis and for spectral analysis of unknown gases. The FTIR technique can also be used in combination with a lamp as a source. The main disadvantage is that FTIR systems depend on a complete scan with a highly refined interferometer, which needs to be hardened for field applications. The correlation spectrometer (COSPEC) has been the main tool for remote monitoring of volcanic SO_2 fluxes. Although attractive for their simplicity, passive instruments require a detailed knowledge of the spectral distribution of the ambient radiation utilized, which often is problematic.

In contrast, active methods use an artificial radiation source, which can be either a classical broadband lamp or a narrowband laser, depending on the requirements and measurement method. Differential optical absorption spectroscopy (DOAS) normally uses a broadband light source, and it is mainly used for integral measurements over long optical paths in the atmosphere. A variety of the technique works in the passive mode and uses the sky as a background source [8]. The DOAS technique is widely applied for measurements of urban pollution levels, e.g., NO_2, SO_2 and O_3 [28,29]. Broadband optical absorption is not entirely suitable for real-world applications, primarily because of poor selectivity due to the limited resolution.

Laser spectroscopy is frequently the method of choice for *in situ* trace gas analysis, because of its directionality, high spectral brightness (for attaining high sensitivity), and narrow bandwidth (for minimizing interferences). Light detection and ranging (Lidar) provides range-resolved atmospheric measurements in a radar-like fashion, and can be used to monitor aerosols. Differential absorption lidar (DIAL) allows species specific measurements of most atmospheric trace gases (including for example SO_2 and Hg) [30,31].

Tunable diode laser absorption spectroscopy (TDLAS), performed in the remote-sensing mode, provides an alternative. The first atmospheric measurements by TDLAS used a long-path retroreflector to achieve sufficient sensitivity for CO measurements in cities [32]. TDLAS has already become a standard against which other non-species specific techniques can be compared and calibrated. Tunable diode laser absorption spectroscopy for remote detection and sensing of NO_2 has been pursued within the present work [Paper II].

Lasers can also be employed for aerosol particle sensing, for example in time-of-flight monitoring [5], and light scattering measurements [Paper V]. High reliability and accuracy, and possibility of detection of the particles in their airborne state are some of the main advantages of the scattering technique.

2.3 Technology Deployment

Technology deployment, in this particular case utilization of environmental monitoring techniques and equipment, is affected by several essential factors. A framework of various technical, economical, and societal requirements can be recognized. These complementary, and sometimes concurring, factors have to be properly understood and integrated, in order to ensure effective implementation of technology and achievement of real environmental gains. The diagram in Fig. 2.1 illustrates the interdependencies affecting deployment of environmental technology.

Technical requirements

In industrial and monitoring applications the requirements on gas sensors are: high accuracy (correct concentration), excellent linearity, high sensitivity (low detection limit – at least at concentration levels prescribed by the regulating authorities), good selectivity (free from interferences), versatility (multi-gas compound measurement), real-time and continuous measurement capabilities, easy to integrate and to utilise (no sampling, user friendly, free of maintenance, no skilled operator – unattended automatic measurement). Additionally, operation in industrial environments often means that the equipment must be rugged (insensitive to shocks, noise, contaminants and high temperatures), compact, and flexible. It is particularly advantageous if the

methods and equipment employed are not only reliable, but can also be configured in a self-checking arrangement.

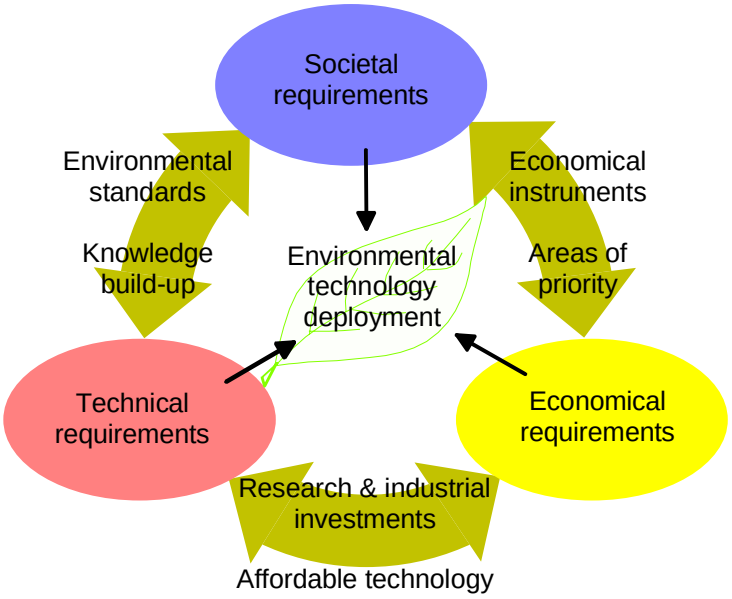

Fig. 2.1 *Environmental technology deployment: requirements and interdependencies.*

Economical requirements

Demand for cost-effective measurement methods and equipment is implicit. Unfortunately, environmental technology has long been perceived solely as a cost, an imposed necessity, monitoring being mandatory to fulfil legislative requirements. Today, industrial plants in many countries are forced to measure their own emissions, and part of their taxation may be dependent on the emission values. The awareness about the beneficial economic aspects of emission monitoring and gas detection is, however, increasing. For example, in the petrochemical industry, searching for and eliminating leaks is of interest from an economical point of view, because it reduces loss of valuable raw material. Industrial process control may result in improved energy efficiency and product quality [33], resulting in fuel savings and more competitive products. Online gas analysis is already used in many manufacturing plants as a vital control tool for sophisticated production processes.

Societal requirements

Health and safety of the public and the operating personnel at industrial plants are directly affected by ambient air quality and gas emissions at workplaces, respectively. Monitoring of environmental status and of gas leaks is therefore of great importance. Easily deployable surveillance techniques for assessing sites of accidents, e.g., involving gas tankers or trains, are desirable for safety considerations.

Episodes of high SO_2 concentrations in the 1950s have stimulated the authorities to adopt anti-pollution laws in cities. Nowadays, no large city is spared by photochemical pollution. In many countries, public demand for improved air quality drives the need to reduce air-pollutant emissions. Increasingly stringent environmental and legislative requirements have stimulated the development and utilization of gas monitoring technology. The measurement of real-world emissions from, e.g., industrial utilities and automobile traffic, is important for evaluating the implementation and durability of emission controls and for the design and evaluation of air pollution abatement strategies. It has been shown that the introduction of measures aimed at minimising pollution, such as allowance trading initiatives and emission limitations (e.g., at power stations through burning low-sulfur coal and flue gas desulfurisation), have led to reductions of total SO_2 and NO_2 emissions in some countries .

Simply the availability of a certain technology is, however, not enough to ensure its deployment [34]. Economic aspects, lack of awareness, incompetent management, and fear – justified or not – of evidence of bad performance which may pose legal implications, are some of the reasons that may hinder real-world application of environmental monitoring techniques. A large responsibility lies on decision-makers, who ought to design effective policies and instruments, and make the use of such technology attractive to the prospective user group. Proper environmental management by the enterprises is also essential. It has been suggested that true optimisation of industrial performance can only be achieved when all the different aspects of production (such as energy efficiency, product quality and environmental performance) are integrated [33].

Another important aspect in achieving sustainable development and improvements in the status of global environmental is to make advanced monitoring and pollution abatement technologies, as well as know-how available also in the developing countries, where it is desperately needed [35]. With the rapid economical development involving production and knowledge build-up in some of the developing countries, there is a unique chance to make such technologies affordable and available worldwide. The Earth is our common home, and environmental pollution and climate change are two very important issues that we ought to solve together.

CHAPTER 3

TUNABLE DIODE LASERS

In 1962, less than two years after T. Maiman operated the first (ruby) laser, four American research groups announced, almost at the same time, that they had achieved laser action in semiconductor junctions [36-39]. These early homostructure diode lasers (made of only one semiconductor material) operated in a pulsed mode at cryogenic temperatures to avoid catastrophic failure caused by heat build-up. When the first double-heterostructure, room-temperature, continuous-wave diode lasers (based on $Al_xGa_{1-x}As/GaAs$) were operated in 1970 [40] at Bell Labs in the USA and by Z. Alferov in Russia [41], their lifetimes were measured in minutes. Diode laser lifetimes have increased dramatically since that time, at present being estimated to be hundreds of years, with a wavelength stability greater than 0.1 nm over a period of 25 years [42].

During the 1980s, driven by the demand in the communication and consumer electronic markets, the diode laser was transformed into a compact, low-prize, and reliable opto-electronic component emitting coherent radiation at room temperature useful for many applications. Except from being used in compact disc players, optical memories, laser printers, bar-code readers, telecommunications, alignment and pointing applications, diode lasers can provide cheap and realistic implementations of techniques developed using more complex and expensive laser sources. In 2000 the Nobel Prize in Physics recognized discoveries concerning the important role of semiconductor heterostructures (including diode lasers) in the development of the information- and knowledge-based society of today.

For comprehensive reviews of diode lasers, their electrical and optical properties, performance characteristics and device materials along with the corresponding manufacturing techniques, the reader is referred to [43-45]. Further information on the physics of semiconductors in general can be found in standard books on solid state physics [46]. Numerous books deal with the basics of laser operation in general and of semiconductor lasers in particular [47,48].

Since the work presented exclusively makes use of moderately powered (5-200 mW) diode lasers emitting visible and near-infrared radiation (around 400 nm, 635

nm, 690 nm, 760 nm, 780 nm and 980 nm), the following presentation will focus upon these diode types and their application in spectroscopy.

3.1 Diode Laser Characteristics

Generally, each diode laser architecture and each device has its own characteristics. Therefore, each individual diode must be tested before it can be utilized in a specific application.

3.1.1 Fundamentals

The typical diode laser has a dimension of 200×200×400 μm^3. Electronic contacts are evaporated onto the crystal, which is then mounted on a rigid block. The laser has a sophisticated internal structure, based on the double heterostructure architecture, where the active (laser) medium is sandwiched between two other semiconductor materials with higher bandgap energies. Lasing action in a diode laser is achieved by applying a forward bias current (typically 0.1-1.0 A) which injects charge carriers (electrons or holes) across the p-n junction, as shown in Fig. 3.1. This produces population inversion between the nearly empty conduction band and the nearly full valence band, providing the gain mechanism through which stimulated emission occurs via electron-hole recombinations across the bandgap E_g. The emitted photon energy approximately equals the bandgap energy.

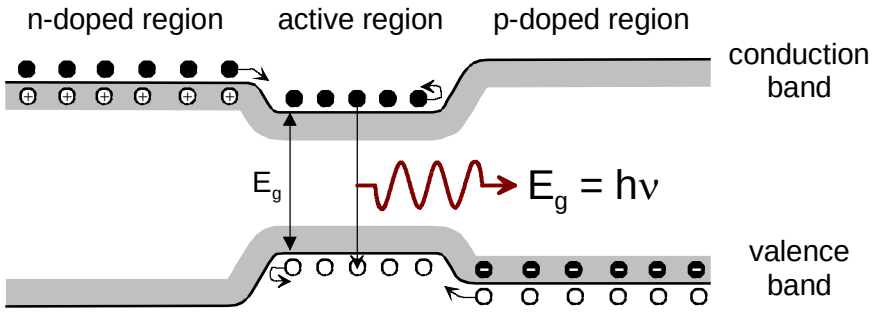

Fig. 3.1 *Energy band diagram of a p-n junction. Recombination of electrons and holes across the bandgap generates the laser radiation.*

The optical resonator needed to insure continuous laser action is formed by cleaving the facets of the semiconductor material along natural crystal planes. The difference in refractive index between the semiconductor laser material (for AlGaAs, n ≈ 3.6) and air (n ≈ 1) yields a reflectivity of about 32%. By applying an anti-reflectance coating on the output facet (typically leaving 2-20% in residual reflection) and a high-reflectance coating on the back facet of the diode laser, higher output powers can be generated. The spatial mode of the laser is defined by a narrow channel in the active region that confines the light. The confinement is achieved by spatial variations in the index of refraction (index guided) of the semiconductor material. An enormous variety of different semiconductor structures has been developed, and is comprehensively covered in [44].

At low currents, diode lasers act as light emitting diodes, since the internal losses are too high to produce population inversion. When the current equals a certain threshold value, the diode starts to emit coherent light. Above the threshold, the laser output power varies linearly with current. The electro-optical conversion efficiency is comparatively high, typically 10-30%.

The laser beam profile is elliptical because of the rectangular shape of the emitting surface. Owing to the small cross-sectional dimensions of the active region (about 3 μm × 1 μm), the beam divergence angle can be 30° or more. The cross-section of the beam resembles a Gaussian profile. The output beam from a diode laser is astigmatic, owing to the directional dependence of the refractive indices in the cavity. Since diode lasers are usually sealed by a planar glass window, spherical aberration is introduced when the divergent output beam passes through the window. These factors affect how well the diode laser radiation can be collimated and focused. The construction of a typical commercial diode laser is shown in Fig. 3.2.

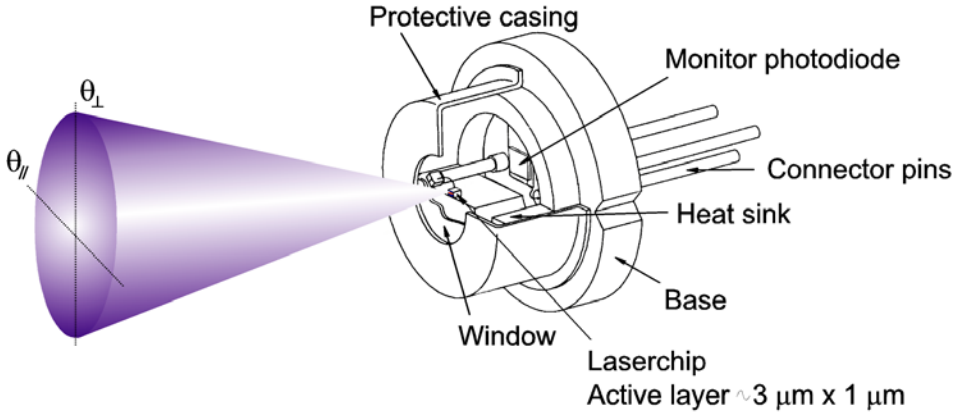

Fig. 3.2 *Diode laser anatomy.*

Most diode lasers emit linearly polarised light along the *p-n* junction plane. The polarisation ratio is typically 100:1 or more when the diode laser is operated near its maximum power. Near the threshold currents the share of unpolarised light due to spontaneous emissions is higher and consequently, the polarisation ratio decreases. Currently, single mode diode laser technology in the visible and near-infrared wavelength region (about 400 nm to 2 μm) offers output powers in the range 5-200 mW.

3.1.2 Wavelength and Tunability

As mentioned previously, the emission wavelength of the diode laser radiation is determined, to a first approximation, by the bandgap of the semiconductor material, which in turn depends upon the composition of the crystal (choice of alloy material and stochiometric composition). Commercially available room-temperature-operated diode lasers operating in the ultraviolet, visible, and near-infrared region (0.37-2.00 μm) are based on group III (Al, Ga, In) and group V (N, P, As, Sb) semiconductor materials. The available emission wavelengths are almost exclusively dictated by the demands on the telecommunication and consumer electronic market. For example, telecommunication diode lasers are manufactured to cover the important wavelength range around 1.3 μm and 1.55 μm, corresponding, respectively, to the lowest material dispersion and loss in optical fibers.

The Fabry-Pérot resonator formed by the crystal end facets defines the resonance conditions for laser emission, which occurs in a series of longitudinal modes separated by

$$\Delta\nu = \frac{c}{2nL}, \tag{3.1}$$

where ν is the laser frequency, c is the speed of light, n is the refractive index of the semiconductor material, and L is the cavity length. The typical longitudinal mode spacing is around 150 GHz (using $n = 3.6$ and $L = 300$ μm). Semiconductor diode lasers oscillate essentially in several longitudinal modes because the gain spectrum linewidth of the semiconductor material is much broader than the separation between adjacent longitudinal modes. Depending on the processing technology and the wavelength, diode lasers feature more or less multimode behaviour. For example, index-guided diode lasers typically emit light in a single longitudinal mode. A benefit of the small lateral dimensions of the active region is that it ensures an essentially single transverse mode emission. The linewidth of a single mode diode laser is extremely narrow (10-100 MHz) and well characterized by a Lorentzian [49]. The minimum linewidth is determined by fundamental spontaneous emission fluctuations and gain-index coupling in semiconductor materials. Temperature and current instabilities can increase the linewidth to several hundred MHz.

One of the most useful features of diode lasers, making them useful in atomic and molecular spectroscopy, is their wavelength tunability. The wavelength can be tuned by altering the temperature or by varying the injection current. The laser wavelength tunes with temperature because both the optical path length of the cavity (physical length and refractive index, $L \times n$) and the gain curve (energy bandgap) depend upon crystal temperature. However, these two temperature dependencies are quite different; e.g., in an AlGaAs diode laser, the gain curve tunes ~0.25 nm/°C and the change in the optical path length of the cavity tunes ~0.06 nm/°C. Tuning by current, which involves ohmic heating of the active region only, causes a change in the refractive index of this region (due to change of the carrier density), which in turn produces a change in wavelength.

Temperature or current tuning of the diode results in a series of continuous tuning ranges, typically 20-80 GHz wide, separated by gaps where no emission occurs, a phenomenon known as *mode hopping*. Due to this behaviour there are some wavelengths, which are not accessible at all. The exact location of a mode hop can sometimes be remedied by choosing a different combination of base temperature and injection current. The maximum continuous tuning range corresponds approximately to half the longitudinal mode spacing (the free spectral range) of the diode laser. A typical tuning curve of a single-mode 980-nm Fabry-Pérot diode laser is displayed in Fig. 3.3. The slope of the continuous portions corresponds to the tuning of the lasing longitudinal mode, while the mode hops correspond to a shift between different longitudinal modes (not necessarily neighbouring ones), caused by the shift in the gain curve.

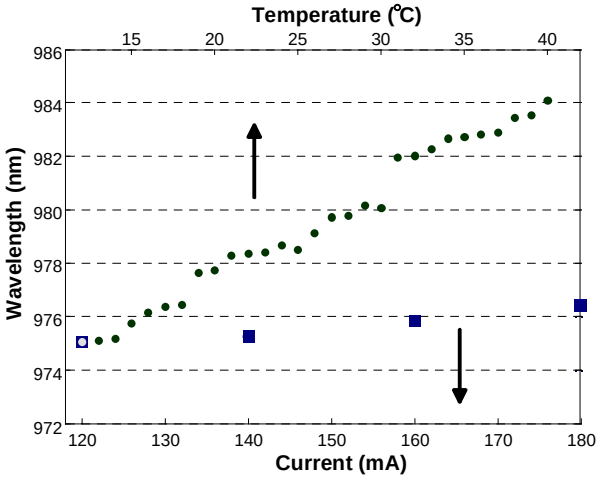

Fig. 3.3 *Variation of the wavelength output of a Fabry-Pérot single-mode diode laser with current (filled squares, lower horisontal scale) at a temperature of 12 °C; and with temperature (filled circles, upper horizontal scale) at a current of 120 mA. The maximum continuous tuning range for this diode laser is about 0.16 nm (50 GHz).*

3.1.3 Modulation

Diode lasers can be modulated very rapidly (up to 10 GHz) by changing the injection current. Thereby *amplitude modulation* (AM) of the light intensity is achieved, an application used in, e.g., optical fibre communications, where light is switched on and off very rapidly to convey information. The possibility to generate very short light pulses was employed in temporal resolved measurements in Paper VII. However, as discussed in the previous section, current modulation changes also the wavelength (and frequency) of the emitted light, thereby inducing so called *frequency modulation* (FM). In conclusion, when the injection current is modulated, combined amplitude and frequency modulation is generated with a phase difference between the two. The AM-FM phase shift depends on the laser structure and the modulation frequency.

The frequency modulation capability is particularly useful and can be employed to increase the sensitivity in, e.g., absorption spectroscopy measurements, as further discussed in Chapter 5.

3.2 Extending the Wavelength Range

Although most diode lasers used today are emitting in the visible and near-infrared, there is a constant strive to develop semiconductor compounds that can cover also the mid-infrared and the ultraviolet wavelength regions. Diode lasers emitting in the mid-infrared region (2-30 μm), include lead-salt, antimonide, and quantum cascade laser sources. Most of them require cryogenic cooling for cw operation, but currently, some new lasers can achieve sustained lasing action with only thermoelectric cooling.

Lead salt diode lasers have been available since the mid-1960s. More recently, quantum cascade lasers (QCL) have been developed, and have already found widespread application, also in the field of trace gas monitoring [50]. These lasers are unipolar semiconductor injection lasers designed by means of band-structure engineering in a multiple quantum-well heterostructure. The emission wavelength depends on the thickness of the quantum well and barrier layers of the active region rather than the energy bandgap. QCLs have been fabricated for emission wavelengths from 3.5-24 μm, have high output power, and operate either in continuous-wave or pulsed mode. Details of their design and operating characteristics can be found in [51,52].

Another diode laser is the Vertical Cavity Surface Emitting Laser (VCSEL). These devices are simpler and more cost effective to produce than their traditional index-guided counterparts, and emit single-mode radiation in the near-infrared region (750-960 nm). VCSELs have a wide tuning range (~30 cm^{-1} or 2 nm) by changing the operating current from threshold to maximum. Their output power, however, is very low (<1 mW). Recently, a development of the VCSEL design, called Novalux

Extended Cavity Surface Emitting Laser (NECSEL), promises higher output power levels [53].

In the following two subsections the blue/violet diode lasers are briefly introduced, and a short introduction to frequency mixing, with emphasis on sum frequency generation, is given

3.2.1 Blue and Violet Diode Lasers

The strive for ever shorter diode laser emission wavelengths, today especially in the blue/violet spectral region, is mainly driven by the consumer and data storage markets, which utilizes the lasers in, e.g., laser printers (photosensitive materials are more sensitive at shorter wavelengths), optical memories (data can be more densely packed), lithographic processes in the semiconductor industry (finer structures can be achieved), and all-diod-laser TV screens (three primary colors are needed).

Since November 1996, when the new technology was successfully demonstrated by S. Nakamura [54], research and development in blue diode laser technology has resulted in much improved overall quality and reliability of the lasers, and increased the available wavelength range. Blue and violet diode lasers are based on gallium-nitride (GaN) or indium-gallium-nitride (InGaN) semiconductor materials, elaborately engineered using nano-technology into a multi-layered structure (composed of 743 different layers of well-controlled thickness), schematically shown in Fig. 3.4. These substrates are currently available to provide radiation in the spectral range of 370–445 nm, with output powers up to 35 mW, and a guaranteed lifetime of 10,000 hours [55]. The spectral properties of the first devices were not very well suited for spectroscopic use, since their emission was longitudinal multimode, and the output beam profile had inferior quality. It is a common phenomenon in the development of diode lasers; the first diode lasers emitting in a new wavelength region exhibit mostly multimode operation, and, eventually, when the processing technology matures, single-mode operation becomes more dominant. Further developments on the diode laser market towards even shorter wavelengths, better reliability, and higher power are most likely to occur.

Part of the work presented here constitutes some of the first spectroscopic applications of these new laser sources, including sensitive frequency-modulation spectroscopy measurements on pollutants [Paper I, III, IV].

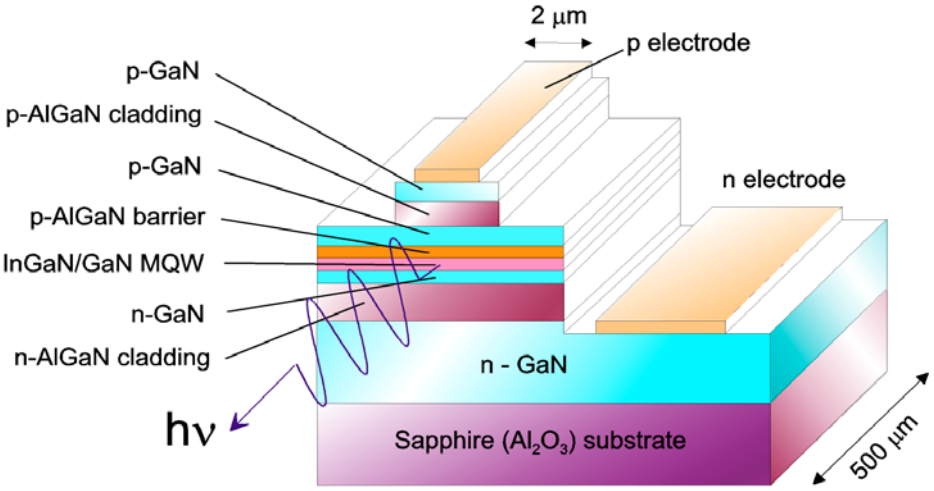

Fig. 3.4. *Schematic view of the multi-layered structure of the gallium-nitride blue light emitting diode laser. The active layer is a multilayer quantum well (MQW) structure.*

3.2.2 Frequency Mixing

The generation of harmonics, sum or difference frequencies, by use of nonlinear optical frequency conversion, can conveniently extend the available wavelength range of diode lasers far into the ultraviolet and the infrared spectral region. For room-temperature-operated diode lasers nonlinear optical frequency conversion – also called *frequency mixing* – is a practical way of producing tunable radiation in this extended wavelength range. A comprehensive description of the different nonlinear optical processes can be found in textbooks in the field [56,57]. In this section, a brief description of techniques related to the present work, especially sum-frequency generation of ultraviolet radiation, is given.

When light of sufficiently strong intensity (mainly laser light) propagates through a nonlinear optical medium, the polarisation of the medium can be expressed as

$$P(t) = \varepsilon_0(\chi^{(1)}E(t) + \chi^{(2)}E^2(t) + \chi^{(3)}E^3(t)+\ldots), \tag{3.2}$$

where E is the applied optical field, ε_o is the permittivity of free space, $\chi^{(1)}$ denotes the linear susceptibility, and $\chi^{(2)}$, $\chi^{(3)}$, ... are the nonlinear optical susceptibilities. The first term in Eq. 3.2, the linear polarisation, is responsible for ordinary optical phenomena, such as reflection and absorption, while the second term, the second-order nonlinear polarisation, gives rise to difference-frequency, sum-frequency, and second-harmonic generation. This can be realised if one considers an electromagnetic optical field $E(t)$ consisting of two different frequencies ω_1 and ω_2, represented in the form

$$E(t) = E_1 \exp(i\omega_1 t) + E_2 \exp(i\omega_2 t), \tag{3.3}$$

which propagates in a nonlinear medium. The second-order nonlinear polarisation is given by

$$P^{(2)}(t) = \varepsilon_0 \chi^{(2)} \left[E_1^2 \exp(i2\omega_1 t) + E_2^2 \exp(i2\omega_2 t) + 2E_1 E_2 \exp(i(\omega_1 + \omega_2)t) \right.$$
$$\left. + 2E_1 E_2 \exp(i(\omega_1 - \omega_2)t) + c.c. \right] + 2\varepsilon_0 \chi^{(2)} \left[E_1 E_1^* + E_2 E_2^* \right]. \tag{3.4}$$

Thus, four new frequency components are generated: the doubled frequencies (second harmonics) $2\omega_1$ and $2\omega_2$, the sum frequency $\omega_1+\omega_2$, and the difference frequency $\omega_1-\omega_2$. According to the Maxwell equations, these components of the nonlinear polarisation act as driving terms for the generation of an electromagnetic field at the new frequencies. Owing to the fact that efficient generation of new frequency components requires that certain phase-matching conditions between the interacting waves are fulfilled, typically only one frequency component can be optimized to reach an appreciable intensity.

In sum frequency generation (SFG), two laser beams at different frequencies are combined in a nonlinear medium with suitable dispersion characteristics. This generates a beam at the sum frequency. The narrow emission spectra of the driving fields is inherited by the newly generated radiation. The sum-frequency wavelength tuning is accomplished by tuning either of the primary lasers, or both. In order that the generated radiation continues to build up as the beams pass collinearly through the nonlinear material, the three waves must stay in phase (called the *phase matching condition*). This condition can often be satisfied in a birefringent nonlinear crystal (having an *ordinary* n_o and an *extraordinary* n_e refractive index) by proper orientation of the crystal and the polarization of the input radiation. A drawback is that the three waves will generally not propagate in the same direction due to double refraction. The beams will separate as they pass through the crystal (*walk-off*), which will limit the overlap region and the generated power. Partial phase-matching between the interacting waves can also be achieved by using *quasi phase-matching*, in which a periodic structure is built into the nonlinear medium so that the relative phase is corrected in regular intervals [58-60].

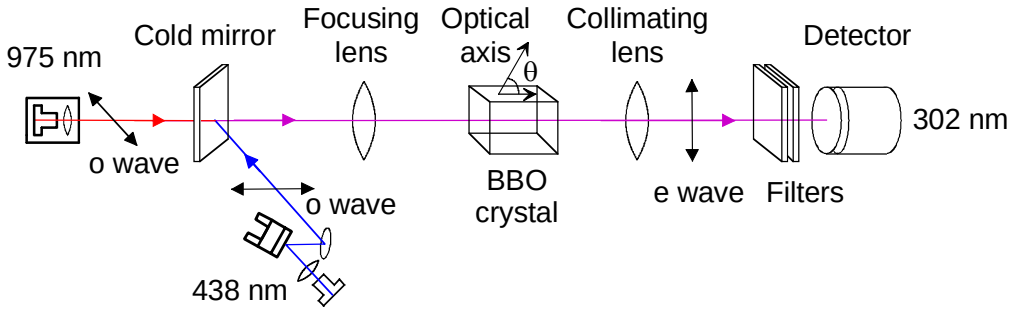

Fig. 3.5 *Experimental setup for sum-frequency generation at 302 nm using type I phase-maching in a BBO crystal. The polarization of the mixing waves is marked with arrows.*

The maximum SFG output power is proportional to the crystal length, power of the primary radiation fields, and the square of the second-order nonlinear coefficient of the crystal. High conversion efficiency is obtained by means of precise spatial overlap and focusing of the primary beams. An optimal focus can be achieved by balancing a tighter focusing against the decrease of interaction length due to diffraction. The general expressions governing the conversion efficiency for sum- and difference-frequency generation are given and discussed in Papers III and [61,62].

Sum-frequency generation is typically employed to convert the radiation from lasers in the near-infrared and visible to the visible and ultraviolet spectral regions. In the present work sum-frequency generation to 254 nm (ω_1 = 404 nm, ω_2 = 684 nm) for mercury detection [Paper III], and to 302 nm (ω_1 = 438 nm, ω_2 = 980 nm) for sulfur dioxide monitoring [Paper IV], have been achieved by frequency mixing in a BBO (β-BaB_2O_4) crystal. Beta barium borate is a negative ($n_o > n_e$) uniaxial crystal, and so called Type I phase-matching, i.e., both primary waves having the same polarization, was chosen. In Fig. 3.5 the experimental arrangement used for SFG of UV radiation at 302 nm is schematically illustrated.

3.3 External Cavity Diode Lasers

Due to the low reflectivity of the cavity facets (typically R $\approx$ 0.32), light emitted from a diode laser can easily be back-coupled into its cavity by an external reflection. The dynamic properties of the laser are significantly affected by the interference between the feedback light and the field inside the primary laser cavity. Sensitivity to optical feedback can be detrimental because it can induce mode hops and interference fringes, as further discussed in Chapter 5.1. However, it can also be exploited to improve the spectral purity and tuning performance of diode lasers.

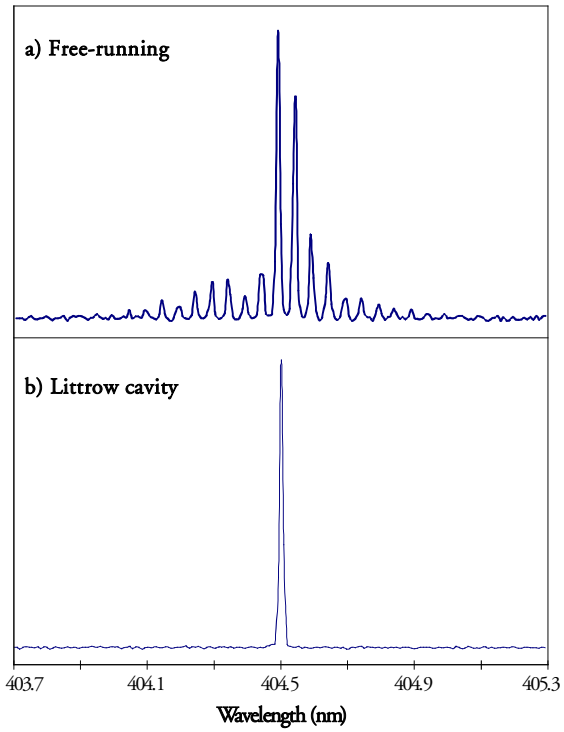

Fig. 3.6 *Output spectra from a blue diode laser operated without (a) and with (b) an external cavity. The poor resolution of the spectrometer used, renders the line narrowing not visible.*

In a so called external cavity diode laser (ECDL) arrangement, optical feedback from, e.g., a mirror or a grating, may force an inherently multimode laser to oscillate on a single frequency. To illustrate the dramatic effect on the emitted spectrum, the output of a blue diode laser with and without an external cavity is shown in Fig. 3.6. External optical feedback may also induce a single-mode laser to tune across the "forbidden" hode hops, or to access a larger wavelength range within the broad gain spectrum of the laser [63]. Mode-hop-free single-frequency tuning ranges of over 1000 GHz have been demonstrated [64]. In addition to longitudinal mode selection and wavelength tuning, an ECDL configuration also narrows the linewidth of the output radiation [65].

Normally, in an ECDL, one or both facets of the laser chip are antireflection-coated to eliminate optical feedback (residual reflection of 10^{-3} or less). Instead, the feedback required for laser action is provided by an external cavity, which acts as a narrow wavelength selector. Several cavity configurations have been developed (Littrow, Littman) that differ in the method of tuning, number of components, output beam characteristics, and output coupling efficiency [66,67]. In the present work, the Littrow configuration has been used in Papers III and IV. All ECDL designs

have been based on tuning of a (dispersive) frequency selector by mechanical means. This requires a very high mechanical stability and careful alignment. Descriptions of the various ECDL configurations are presented in [68].

Another design also utilising the principle of selective wavelength feedback is used in the distributed feedback (DFB) and the distributed Bragg reflector (DBR) diode lasers. In these devices, a frequency selective grating is incorporated into the cavity structure (within or outside the active region), ensuring pure single-mode operation and wavelength tuning without mode jumps. A drawback is that DFB and DBR diode lasers have a limited tuning range of a few nanometers only.

In Paper V, a free-running diode laser (of the same type as used in CD players) was utilized in a coupled-cavity arrangement for aerosol particle detection. Since the output facet of the laser was not antireflection coated, the diode had to be operated below its free-running threshold current in order to achieve stable lasing conditions. The optical feedback from an external low-reflectance mirror was utilized to reduce the optical losses and insure lasing action. This configuration is consequently very sensitive to changes in the optical loss due to, e.g., aerosol particles entering the external cavity and thereby obstructing the optical feedback into the laser. In Appendix A, a simple coupled-cavity model is presented which relates the extinction factor Q_{ext} of an aerosol particle (see Section 6.1.1), to the power decrease inside the coupled cavity [69]. This change in signal can be used to evaluate the optical equivalent size of the particle.

CHAPTER 4

ABSORPTION SPECTROSCOPY

Atoms and molecules may undergo transitions between electronic, vibrational, and rotational levels when exposed to electromagnetic radiation, resulting in absorption spectra. These spectra consist of a manifold of narrow absorption lines, which are unique to each atom and molecule, and present an identifiable "fingerprint" of the gaseous species. Spectroscopic trace gas detection is a powerful method allowing quantitative determination of the concentration, temperature and pressure of a gas, from a measured optical absorption spectrum. In order to evaluate the detected signal one needs a theoretical model that describes the absorption line shape and line broadening mechanisms under varying environmental conditions. These aspects are briefly reviewed in this chapter, and reference to various spectroscopic databases is given. In the final section some important features regarding diode laser use in spectroscopy are discussed. A broad survey of spectroscopic techniques for basic studies and practical applications is provided, e. g. in Ref. [70].

4.1 The Beer-Lambert Law

Laser absorption spectroscopy is based on the Beer-Lambert law. It states that in the absence of optical saturation and particulate-related scattering, the intensity $I(\nu)$ at frequency ν of the light propagating in a homogeneous gas of sample length L[cm] is attenuated exponentially

$$I(\nu) = I_0(\nu)\exp\left[-\sigma(\nu)NL\right], \tag{4.1}$$

where $I_0(\nu)$ represents the original intensity, $\sigma(\nu)$ is the frequency-dependent absorption cross-section [cm^2/molecule], and N is the concentration of the absorbing species [molecules/cm^3]. Often the absorption coefficient $\alpha(\nu)$ [cm^{-1}] is introduced, according to $\alpha(\nu) \equiv \sigma(\nu)N$. Since in trace gas sensing applications the species of interest are often present in very low concentrations, the Beer-Lambert law reduces to

$$a \equiv \sigma(\nu_0)NL \approx \frac{I_{abs}(\nu_0)}{I_0(\nu_0)}, \tag{4.2}$$

where a is the absorbance, $\sigma(\nu_0)$ is the absorption cross-section at the line center (ν_0), and $I_{abs}(\nu_0) \equiv I_0(\nu_0)$-$I(\nu_0)$ is the light intensity absorbed by the gas at that frequency. It is convenient to express the absorption cross section in terms of a line strength S (also refered to as the line intensity) and a normalized line shape function $g(\nu-\nu_0)$ [cm^2], according to

$$\sigma(\nu) = S\,g(\nu - \nu_0), \tag{4.3}$$

where ν_0 is the frequency at the line center.

The overall intensity of an absorption line is given by the line strength S [cm^{-1}/(molecule cm^{-2})], and is the integral of the absorption cross-section over the frequency range of the line,

$$S = \int_{-\infty}^{\infty} \sigma(\nu)d\nu. \tag{4.4}$$

The linestrength of an absorption transition depends on the probability of the transition (calculated by using the quantum mechanical wave functions of the energy states involved), and it is proportional to the population density in the lower-state (according to the Boltzman distribution), thus depending on temperature.

4.2 Absorption Line Characteristics

Each absorption line has a certain linewidth and shape that depends on the conditions under which the measurement is performed, i.e., temperature, pressure, and what surrounds the atom or molecule. Different line broadening mechanisms occur due to phenomena in the medium that perturb the energy levels of the transition, or due to the way in which individual atoms and molecules interact with light. The lineshape function $g(\nu-\nu_0)$ describes the spectral variations of the light interaction with the absorbing species. An important parameter characterizing the lineshape function is the halfwidth at half maximum (HWHM), denoted $\Delta\nu$.

Most fundamental is the natural linewidth, which is due to the finite upper-level lifetime τ, and basically reflects the Heisenberg uncertainty relation [71,72,73]. A finite upper-level lifetime in the range from microseconds to nanoseconds gives rise to a diffuse energy level and thus a broader absorption line. This broadening, of the order of 0.1-100 MHz, has a Lorentzian line shape, and is insignificant compared to

broadening by the other two important mechanisms – thermal motion and collision effects.

Depending on pressure, the line broadening mechanisms can be divided into three main regions. At low pressure (<10 Torr), Doppler broadening dominates due to thermal motion – the corresponding line shape is Gaussian. As the gas pressure increases the effect of collisions starts to dominate (>100 Torr), and the resulting line shape is Lorentzian. At intermediate total pressures, when neither thermal nor collisional broadening dominates, the line shape is best described as a convolution of the two respective line shapes, and it is known as the Voigt profile.

Doppler broadening is described by a Gaussian function according to

$$g_D(\nu-\nu_0)=\frac{1}{\Delta\nu_D}\sqrt{\frac{\ln 2}{\pi}}\exp\left[-\frac{\ln 2(\nu-\nu_0)^2}{\Delta\nu_D^2}\right], \tag{4.5}$$

with a halfwidth $\Delta\nu_D$ given by

$$\Delta\nu_D=\nu_0\sqrt{\frac{2kT}{Mc^2}\ln 2}=3.581\times10^{-7}\,\nu_0\sqrt{\frac{T}{M}}, \tag{4.6}$$

where T is the absolute temperature, M is the molecular mass, k is the Boltzmann constant, and c is the speed of light. Hence, the Doppler broadening increases with increasing temperature.

Collisions between the absorbing gas species shorten the effective upper-level lifetime through collisional de-excitation, which leads to a Lorentzian line shape given by

$$g_L(\nu-\nu_0)=\frac{\Delta\nu_L}{\pi}\frac{1}{(\nu-\nu_0)^2+\Delta\nu_L^2}, \tag{4.7}$$

with a halfwidth $\Delta\nu_L$ that depends on pressure according to

$$\Delta\nu_L=\sum_i \gamma_i p_i, \tag{4.8}$$

where γ_i are the pressure broadening coefficients [cm^{-1}/atm] and p_i the partial pressures [atm] of the species present in the absorbing volume. Consequently, both self-broadening from the gas species probed and foreign-gas broadening due to other gases present contribute to the linewidth. For trace gases present in the atmosphere in very low concentrations, air-broadening is dominant. The collision-induced linewidth depends also on temperature according to

$$\Delta\nu_L(T)=\Delta\nu_L(T_0)\left(\frac{T_0}{T}\right)^n, \tag{4.9}$$

where T_0 is a reference temperature (typically 273 K), and the power n is a gas- and a transition-specific parameter (~0.5).

In the pressure range between 10-100 Torr, known as the Voigt regime, the line shape is described by a convolution of Doppler and pressure broadening. The Voigt function tends at high pressure to a Lorentzian and at low pressure to a Gaussian. The Voigt line profile has to be computed numerically [74], and there is no exact formula for the Voigt halfwidth $\Delta\nu_V$. An empirical relation has been given [75]

$$\Delta\nu_V = 0.5346\Delta\nu_L + \sqrt{0.2166\Delta\nu_L^2 + \Delta\nu_D^2}\,, \tag{4.10}$$

but frequently it is sufficient to use a quick estimate provided by

$$\Delta\nu_V = \sqrt{(\Delta\nu_D^2 + \Delta\nu_L^2)}\,. \tag{4.11}$$

Figure 4.1 compares Gaussian (Doppler) and Lorentzian (collisional) lineshapes that have the same linewidth and the same area (equal to unity). The Gaussian lineshape has a peak value that is about 50% higher than the Lorentzian, but it drops off much faster in the wings.

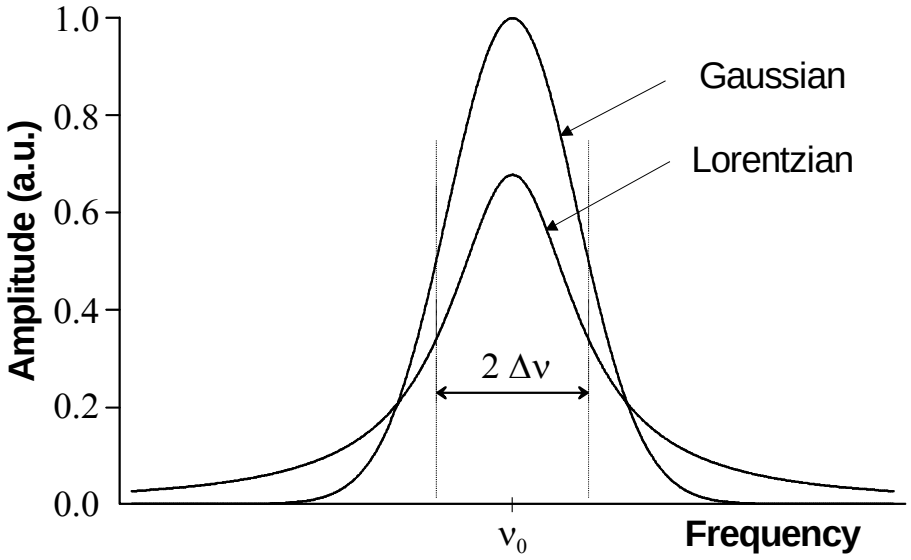

Fig. 4.1 *Comparison of Gaussian and Lorentzian lineshapes with the same HWHM.*

In standard environmental conditions, i.e., at ambient temperature and atmospheric pressure, the Doppler contribution to the overall linewidth can often be neglected, and the line shape be treated as pure Lorentzian. At these conditions, pressure-broadened linewidths are typically on the order of 0.1 cm^{-1} (3 GHz), which is

larger than the Doppler width. This excessive broadening results in progressive overlapping and blending of the molecular absorption lines of many larger molecules. Generally, it can be said that the contrast between the line absorption and the background decreases with increasing pressure. Conversely, at pressures low enough, the line shape can be treated as pure Gaussian. This is the case, e.g., when low-pressure gas cells are used, as in the Papers I and III. Comparisons between low and atmospheric pressure spectra are shown for mercury in Fig. 4.2(a), and for sulfur dioxide in Fig. 4.2(b). The recordings illustrate the increased signal peak sensitivity at reduced pressure, although the integrated absorbance remains constant.

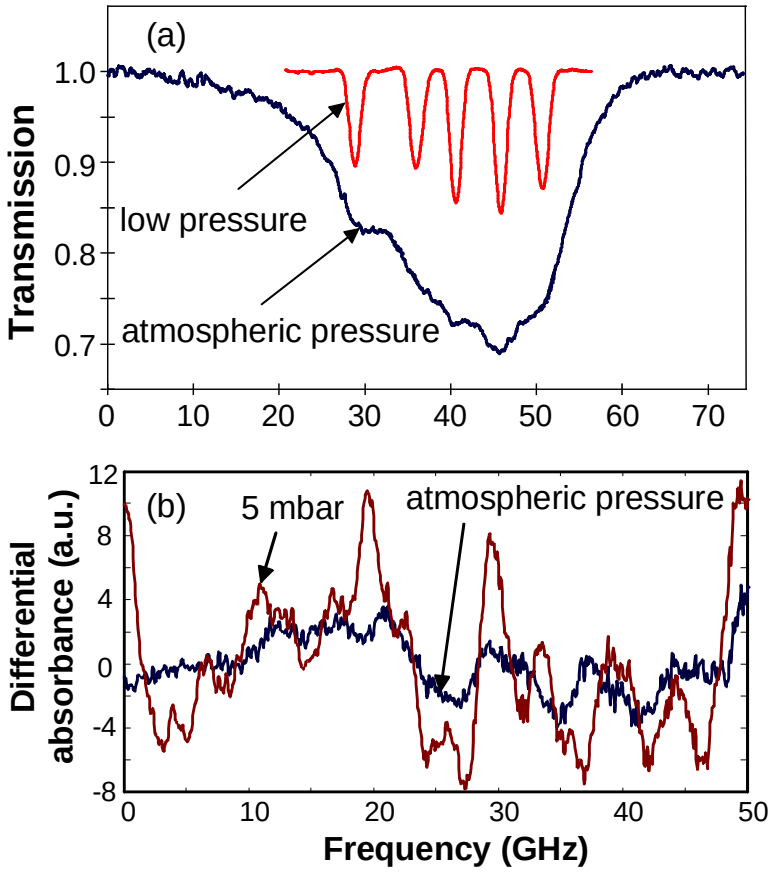

Fig. 4.2 *High resolution spectra of (a) mercury measured at 254 nm and of (b) sulfur dioxide of 30 ppm-m concentration recorded at 302 nm obtained with different diode-laser-based spectrometers. Comparison between low pressure and atmospheric broadened spectra show how closely spaced lines progressively overlap at increased pressure.*

The above mentioned recommendations should be used with care, since the actual profile to be used is also largely affected by which particular molecule and transition is studied. This can be exemplified by molecular oxygen, which for the transitions around 760 nm, studied in Papers VI-IX, has a Doppler width of 0.014 cm^{-1} (M=32) and a pressure broadened linewidth of about 0.05 cm^{-1}. This means that the Voigt profile better characterizes this absorption feature. In contrast, the mercury line at 254 nm, studied in Paper III, has a Doppler width of 0.0017 cm^{-1} (M=200) and a pressure broadened linewidth of about 0.11 cm^{-1}, thus being accurately described by the Lorentz profile.

4.3 Absorption of Atoms and Molecules

When choosing an absorption line for trace-gas-detection applications there are three especially important factors to consider:

- The line strength of the absorption line (affects sensitivity),
- The interference from other species (affects selectivity), and
- The linewidth of the absorption line (affects both sensitivity and selectivity).

A strong, isolated, and narrow absorption line is the prefered measurement situation and will most likely yield a high sensitivity and selectivity. This situation is, however, not always possible to achieve. Different aspects regarding detection sensitivity are further discussed in Chapter 5.

Many atomic species have strong transitions in the ultraviolet and visible wavelength regions, where many atomic spectroscopy experiments have been performed. In the present work, potassium, lead, and mercury, absorbing at 404 nm, 406 nm and 254 nm, respectively, have been studied [Papers I and III]. As an example, Fig. 4.3 shows a simplified Grotrian diagram depicting the $4s\ ^2S_{1/2} - 5p\ ^2P_{1/2}$ transition at 404.8 nm in potassium. This transition was probed using a blue diode laser. Even the hyperfine splitting of the ground ^2S state is small because of the small magnetic moment of the ^{39}K nucleus, and was not resolved in Doppler-broadened (800 MHz) absorption measurements. Atomic diode laser spectroscopy is discussed and reviewed in [76].

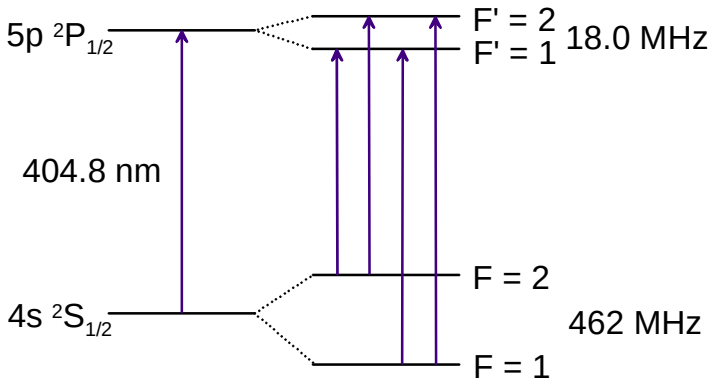

Fig. 4.3 *Hyperfine energy levels of the $4s\ ^2S_{1/2} - 5p\ ^2P_{1/2}$ transition at 404.8 nm in ^{39}K. The energy splittings are not given to scale.*

The largest molecular linestrengths occur in the mid-infrared region (2-15 μm), where all polyatomic molecules, with the exception of the homonuclear diatomic molecules (e.g., N_2 and O_2), have fundamental rotational-vibrational transitions. For example, sulfur dioxide absorbs strongly at 8.6 μm and 7.3 μm; nitrogen dioxide at 6.2 μm and 3.4 μm [77]. The strong molecular absorption bands in this wavelength region make QCL and lead salt diode lasers especially attractive for trace-gas spectroscopic applications.

Overtone and combination lines can be probed in the near-infrared region (0.7-2.5 μm), however, with significantly lower intensities as compared to those for the fundamental vibrational bands. Modulation techniques are frequently used to compensate for this decrease in sensitivity (see Section 5.2). Molecules that absorb in these regions include NH_3 (1515 nm), C_2H_2 (1530 nm), CO and CO_2 (1570 nm), CH_4 (1650 nm) [77].

Transitions between electronic states of atoms and molecules occur in the ultraviolet (UV) and visible spectral region. Especially in the UV (200-400 nm), these transitions can be one or two orders of magnitude larger than the mid-infrared transitions. For example, both NO_2 and SO_2 have pronounced and strong band spectra in this wavelength region with very sharp spectral structures visible only at high spectral resolution [78, Paper IV]. In Fig. 4.4, the nitrogen dioxide spectrum in the region 238-670 nm (measured using a Fourier transform interferometer) is shown.

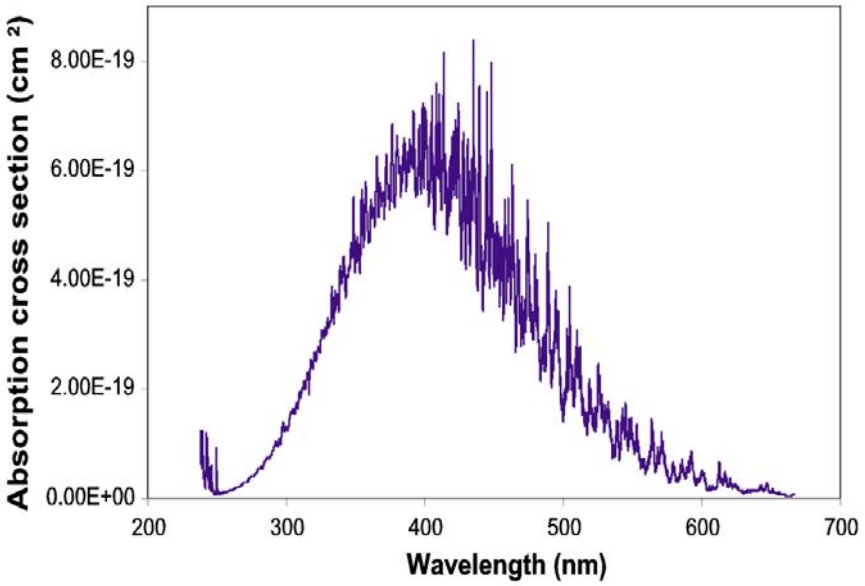

Fig. 4.4 *Absorption cross sections of nitrogen dioxide measured with a spectral resolution of 2 cm*$^{-1}$ [79].

The large amount of trace gases in the atmosphere can cause interference problems, especially in the mid-infrared spectral region. In this wavelength region the absorption coeffiecients of most molecules are very large, which requires very high spectral resolution to avoid interferences between species. In remote sensing experiments, particularly the pressure-broadened lines of the ubiquitous water and carbon dioxide, which are present in large concentrations, render some regions of the spectrum completely opaque, leaving only certain so-called "windows". These windows extend approximately in the ranges from 300 nm (due to O_3) to 1.5 μm, 3-4 μm, 4.5-5 μm, and 7-14 μm. The exact extent is dependent of the detection range and acceptable attenuation. Since relatively few molecules absorb in the near-infrared (NIR) region, there is much less chance for mutual interferences. An additional advantage of choosing this wavelength region is that the ratio of pressure to Doppler broadening is frequently not as large as in the mid-infrared region. Ultraviolet absorption spectroscopy offers several potential advantages, including the absence of significant interference by water vapor and solar-blind detection.

Molecular spectroscopic parameters have been measured and calculated for many atmospheric gases, and are compiled into extensive databases such as HITRAN [77], GEISA [80], NIST [81], IUPAC [82], and PNNL [83]. The most popular is the HITRAN, which currently covers more than one million transitions in the spectral range 0-23000 cm^{-1} and includes data on 37 different atmospheric gases (for example:

H_2O, CO_2, O_3, NO_2, SO_2, CO, CH_4, O_2, OH, NH_3, etc). By using parameters such as isotopes, transition frequency, linestrength, transition probability, line broadening effects, and temperature coefficients; numerically accurate absorption spectra for the different species can be computed. A detailed theoretical description of molecular levels and transitions can be found in [84]. Another valuable source of molecular spectroscopic data, including recent updates to the different databases, is the *Journal of Quantitative Spectroscopy and Radiative Transfer*.

The work presented in this thesis considers near-infrared (760 nm), visible (635 nm, 400 nm), and ultraviolet (302 nm, 254 nm) spectroscopy, using readily available, mostly low-cost, room-temperature operated diode lasers. In Paper II, nitrogen dioxide was monitored in free atmosphere by using an ordinary DVD-player-type diode laser emitting at 635 nm. A more advantageous detection, pursued in the present work in connection to the sum-frequency scheme of Paper IV, is achieved around 400 nm, where much stronger lines are present. Since the molecular transitions in the visible and near-infrared are weak, use of sensitive detection techniques is needed, as further discussed in the next chapter.

An important aspect that should be considered in absorption spectroscopy is the difference in measured line intensity of atoms and molecules. While atomic transitions occur between well-defined electronic energy states, molecular transitions involve a large number of rotational-vibrational components, which means that the measured line strength of atoms is in the order of 10^3 larger than that of molecules. For example, the atomic mercury absorption line at 254 nm (studied in Paper III) allows much more sensitive detection than detection of mercury chloride ($HgCl_2$), under the same measurement conditions.

4.4 Diode Laser Spectroscopy

Ever since tunable diode laser absorption spectroscopy (TDLAS) for atmospheric measurements was first introduced for urban carbon monoxide sensing using a long-path retroreflector [32], the method has gained increased popularity and found applications to gas analysis of a large range of atmospheric species. The diode laser is a fantastic tool for spectroscopy, and its operation characteristics necessary to consider in spectroscopic applications have been discussed in several review papers with respect to atomic and molecular physics, and gas species detection [85,86]. Here, some important aspects of diode laser spectroscopy are briefly presented; first some major features of the technique are considered; then, wavelength tuning and related issues are discussed; and finally, auxiliary equipment and calibration issues conclude this section.

Advantages

One of the most important characteristics of diode lasers for atomic and/or molecular spectroscopy is their wavelength tunability, which allows line by line measurement. The spectral sharpness of diode lasers (10-100 MHz) matches well the narrow absorption linewidth of gases. By rapidly tuning the laser wavelength over single or multiple absorption lines of the species under investigation, high sensitivity, good specificity, and fast response in the measurements are obtained. Similarly to other high-resolution laser techniques, TDLAS allows isotope selective measurements, as demonstrated in Paper III on mercury measurements. As will be discussed in the next two chapters, the excellent modulation capabilities of diode lasers allow implementation of high-sensitivity techniques, as well as temporally resolved measurements.

Diode lasers are easy to implement in real-world applications, being compact and rugged, easy and reliable to operate, having low power consumption, long lifetime, and operating at room temperature. Additionally, they can make use of fibre-optic technology and inexpensive auxiliary equipment, such as low-noise current sources and detectors, thermoelectric coolers, visible optics, etc. Owing their versatility, diode lasers can easily be integrated in miniaturized opto-electronic devices. Especially visible and near-infrared diode lasers, are relatively low-cost, readily available consumables, benefiting from the high manufacturing capabilities of the telecom and consumer market industries.

Drawbacks and remedies

Although diode lasers are well suited for spectroscopy, they still have some limitations for certain applications. For example, all free-running diode lasers have a relatively small continuous tuning range and some also exhibit longitudinal multimode behaviour. The mode-hop behaviour of diode lasers makes a large portion of the total wavelength range potentially covered by a particular diode laser inaccessible. Additionally, the laser wavelength is very sensitive to thermal and current instabilities. These issues, as well as wavelength instability due to mode competition are considered and tackled in Paper IX. Improved wavelength control can be achieved, e.g., by using external cavity schemes, as discussed in Section 3.3. It should be noted that multimode behavior of a diode laser in an absorption measurement on free atoms – although not desired because it reduces spectral contrast and prevents the use of Beer-Lambert's law – does not influence the spectral appearance of isolated spectral features, as shown in experiments studied in Paper I. This is because only one of the oscillating modes at the time interacts with the atoms. In contrast, for molecules with a multitude of close-lying lines, multimode behavior is unacceptable.

Although different combinations of semiconductor materials theoretically allow diode laser operation in the whole range from 370 nm to 30 μm, commercially available diode lasers are in practise limited to a number of specific wavelengths. Diode

lasers operating at new wavelengths are, however, constantly appearing on the market, as discussed in Section 3.2.

Some other practical limitations in the use of diode lasers are: limited power (up to 200 mW for single stripe units), sensitivity for electrostatic transients and mechanical vibrations, and inferior beam quality. Owing to new technological advances the available output power is steadily increasing, while the sensitivity issues and beam quality can be effectively addressed in most applications.

The spectroscopic toolbox

When a spectroscopic experiment is being prepared, normally the first task is to select the proper combination of base temperature and injection current (the working point of the diode laser) at which the laser produces a strong, preferably single-mode emission, that can be tuned to an absorption line of the species under investigation. Since this is frequently more easily stated than performed, because the laser might mode hop or operate in a multimode, it is advisable to purchase several diode lasers for testing, to ensure proper measurement conditions.

As discussed in Section 3.1.2, the wavelength of a diode laser can be tuned by altering the temperature or by varying the injection current. Typically, coarse wavelength tuning is achieved by changing the temperature around the diode laser capsule, while fine tuning is realised by changing the current. For practical reasons, the laser temperature is normally varied using a Peltier element in close connection to the diode laser capsule between 5-50°C, yielding a typical total wavelength coverage of about 10 nm. The lower temperature limit usually prevents water condensation if the diode is exposed to air, and the upper temperature limit prevents thermal degradation which significantly shortens the diode laser lifetime.

A wavelength scan over an absorption profile is usually performed by superimposing a current waveform (such as saw-tooth, rectangular, sinusoidal) at high repetition rates on the operating current of the diode laser. The wavelength is repetitively scanned allowing real-time monitoring of the signals. A special technique called *jump-scanning*, uses a waveform with current jumps that allows fast measurement of multiple transitions in different gas species [87]. The current scan is limited by the threshold and the maximum current values, respectively, and should ensure that the wavelength is scanned continuously across the whole absorption feature of interest (normally > $1cm^{-1}$).

In order to reduce the noise and achieve a high signal-to-noise ratio (SNR), most TDLAS measurements include fast scanning of the diode laser at frequencies around 100 Hz, and subsequent detection of the resulting direct absorption spectrum using a signal averager [88]. By integrating the spectrum a sufficient number of times, the noise can be reduced. The method, referred to as *sweep integration*, provides a measure of the direct absorption and has a detection sensitivity as good as 10^{-5}-10^{-6}. Noise reduction techniques are further discussed in Chapter 5. The signal-to-noise ratio can

be improved by accumulating the signals over periods from ~0.1 s to many minutes depending upon the time response and sensitivity desired. The sensitivity should from a purely statistical point of view increase as the square root of the integration time. but this requires that the laser frequency does not drift. Stabilization of the laser emission can be achieved by locking the working point frequency of the diode laser to the absorption signal from a reference cell containing a high concentration of the target gas (by means of temperature or current change).

Although temperature tuning by a Peltier element is slow – because the inertia of the heat transfer from the heat sink to the semiconductor chip – due to the larger wavelength scan that can be achieved, this mode of tuning may in some cases be preferred, as in the scheme presented in Paper IX. A very fast and effective temperature tuning can be achieved by photothermal heating [89]. An external high-power diode laser (emitting at another wavelength) is focused on the chip of the diode laser to be tuned, producing a heat-inducing wavelength change. Hence, rapid wavelength tuning of the diode laser can be achieved by periodically modulating the high-power laser output. A wavelength scan across several oxygen absorption lines near 760 nm achieved by photothermal heating is shown in Fig. 4.5.

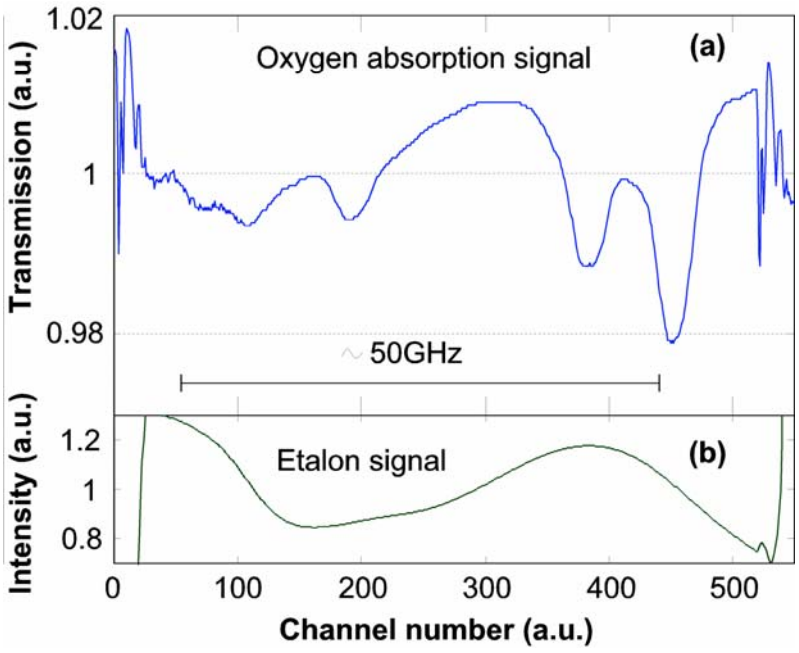

Fig. 4.5 *(a) Oxygen absorption signals near 760 nm obtained by photothermal tuning of a diode laser using a pulsed high-power diode laser (λ = 980 nm) modulated at 4 Hz. The absorption path length was 4 m in air. (b) Etalon signal ($\Delta\nu_{FSR}$ = 50 GHz) shows the non-linear frequency sweep.*

When performing spectroscopic measurements on atoms, a very narrow laser linewidth is required (in the order of 0.1-100 MHz), especially in the case of high-resolution Doppler-free experiments such as saturation spectroscopy. Frequently, a free-running diode laser will not be sufficient, and an external cavity diode laser has to be used to reduce the laser linewidth. A narrow linewidth of the light source is required not only to achieve the desired spectral resolution, but it is also important for accurate quantitative determinations. The recorded linewidth is always a convolution of the linewidth of the laser and of the absorption line. The Beer-Lambert law is fulfilled only if the diode laser radiation linewidth is small compared with the linewidth of the probed species (a rule of thumb is at least a factor of ten smaller). A typical single-mode diode laser linewidth of the order of 10-100 MHz is in most cases sufficient for performing accurate absorption spectroscopy measurements on Doppler- and pressure-broadened molecular lines.

In the following, some auxiliary equipment usually required to perform TDLAS is listed and briefly commented:

- Low-noise diode laser current source (stability <0.05 mA) with protective circuits that prevent electronic transients from deteriorating the laser. Since the drive voltage for a diode laser is in the range of 3-5 V, battery driven current sources can be used with very low noise figures.

- Temperature stabilizer (stability ~0.001 °C) that controls a Peltier element closely attached to the diode laser capsule.

- Frequency stabilizer that locks the working point frequency of the laser to an absorption line of a reference species. This is sometimes needed since drifts induced by temperature fluctuations of, e.g., the surrounding or the equipment used, are very difficult to avoid.

- Low noise current wave generator for tuning the diode laser wavelength. For use in sensitive modulation schemes, additional electronic equipment is needed, such as pulse generators, lock-in amplifiers, mixers, filters, and amplifiers.

- Optics for collimation of the highly divergent beam emitted from the diode laser. Frequently, a moulded glass aspheric lens with a high numerical aperture (typically 0.5 or better) and a short focal length (1-10 mm) is used to minimize the spherical aberrations. If the beam profile is a concern, one can use an anamorphic prism pair to circularize the beam. Unwanted external feed-back into the laser can be reduced by use of an optical diode (see Paper III). Neutral-, color-, interference-, and polarizing filters are used to attenuate, filter, and polarize the light, or to reduce the background. Lenses, mirrors and beamsplitters are used to focus and direct the laser beam. Optical fibers are used to conveniently guide the light.

- Nonlinear crystals to be used in frequency conversion schemes.

- Photodetectors with appropriate bandwidth and spectral sensitivity. Most frequently, semiconductor photodetectors are employed, with wavelength sensitivities dictated by the semiconductor material used; in the visible and near-infrared range: InAs and InGaAs (1-3.5 μm), Ge (0.8-1.8 μm) and Si (< 1 μm). Extremely high sensitivity (single-photon detection) and large dynamic range can be achieved by use of a photomultiplying tube (se Papers III, IV, and VI-VIII). Generally, the longer the wavelength, the more difficult it is to find suitable detectors, which is a particular problem for mid-infrared absorption spectroscopy. For non-visible infrared radiation, the alignment procedures are facilitated by the use of infrared viewers and cards (or of guiding visible laser beams). When high modulation frequencies are applied to the laser light, a main requirement is that the detector area must be small.

- Low-noise preamplifiers for electronic signal amplification and filtration.

- Absolute and relative laser frequency calibration devices. Usually, a wavemeter is used for absolute wavelength calibration. The relative frequency scale can be obtained, e.g., by using a solid (low-finesse) Fabry-Pérot etalon with a free spectral range smaller than the linewidth of the absorbing feature.

- Gas cells and gas handling systems for sampling, calibration and background measurements.

- Data acquisition system with sufficient time response and digital resolution. Computer hardware and software to control the system and for evaluation, display, and storage of data.

Concluding this section, a few aspects of the data evaluation and the determination of the gas concentration are discussed.

As discussed previously, the concentration of the absorbing species can be evaluated from the recorded direct absorption signal using the Beer-Lambert law if the optical path length and the absorption cross-section are known. However, since the direct absorption signal usually is very small ($<10^{-3}$) and the noise might be high, one has to use more sensitive techniques, which often require a separate calibration procedure (see Chapter 5). The system is calibrated by use of a reference cell with a known concentration of the target gas. It is often not necessary to know exactly which absorption line is being monitored. Because of the linearity of the TDLAS technique at low optical densities, usually a single point calibration is sufficient. This can be implemented, e.g., by using the so called *standard addition* method (employed extensively in Papers II, VI-VIII), where known amounts of the calibration gas are added to the unknown ambient air concentration, providing an absolute reference. If possible, the concentration of the "spike" should be chosen to provide an increase in measured concentration comparable to the concentration of the gas in the ambient air.

It should be noted that the accuracy in the determination of the ambient gas concentration is dependent on the accuracy of the calibration gas concentration. This can be problematic, e.g., when diluting standard gas mixtures or when handling corrosive gases (such as nitrogen dioxide) whose integrity in steel containers is not reliable.

During the final evaluation procedure, the recorded data usually first undergoes some primary processing, where, e.g., the background is subtracted, and filtering functions are applied. Since the TDLAS method essentially operates on a differential absorption principle, a broad background does not contribute to the measured absorption signal. Because measurements of trace gases are performed at ambient pressure, the recorded spectra must be properly deconvoluted with respect to different broadening effects, as well as possible interferences. Temperature and pressure conditions can thus be inferred. Consequently, simple intensity ratios or more advanced data evaluation techniques, such as full multivariate analysis of the spectra, can be employed to obtain the gas concentration.

CHAPTER 5

SENSITIVE DETECTION

Comparison between sensitivities of various trace gas sensors can be performed by determining the minimum detectable concentration, e.g, in parts per billion (ppb), for the target molecule, obtained for a given sampling and acquisition time. In the case of a tunable diode laser absorption spectrometer, this translates into a minimum detectable absorbance (see Eq. (4.2)) per pathlength, which pertains for the specific measurement conditions. The minimum absorbance is specified for a signal-to-noise ratio (SNR) equal to 1, and, usually, for a detection bandwidth of 1 Hz. Hence, for TDLAS systems, sensitivity is determined by the minimum detectable fractional absorption that is distinguishable from noise.

In order to achieve high detection sensitivity, i.e. to be able to quantify extremely low trace gas concentrations, two different strategies can be pursued:

(1) reduce the noise, or

(2) enhance the signal at the output of the detection system.

As will be discussed in Section 5.1, noise has different origins, because the measurement system is influenced both by external environmental noise and by intrinsic noise originating from the system itself. Although the causes of noise can only seldom be really eliminated, the basic idea is to reduce the susceptibility of the measurement system for unwanted influence, in order to minimize the amount of noise at the detection side. Many techniques have been developed to achieve noise reduction, e.g., fast scanning [88], balanced beam and balanced ratiometric detection [90,91], and various modulation techniques [92-94]. Each of these high-sensitivity-detection techniques has their own advantages, and the technique used should be chosen depending on the specific application and measurement conditions.

Another option to increase the sensitivity is by enhancing the detected signal, i.e., the absorbance. From the Beer-Lambert law, as expressed in Eq. (4.2), it can be seen that a straight-forward way to achieve signal enhancement is to increase the sample optical path length. This method will be further discussed in Section 5.3. From Eq. (4.3) we recognize that high sensitivity can be obtained by choosing a transition with a

large linestrength (as discussed in Section 4.3). Additionally, narrowing the linewidth of the absorption line by reducing the pressure broadening, is beneficial in increasing the detection sensitivity. Although the integrated absorbance remains constant, the peak absorption, which is inversely proportional to the linewidth, will increase. In fact, the reduction in linewidth will also increase the specificity, since the overlap between closely spaced lines is reduced. This is clearly illustrated in the study of mercury isotopes (Paper III), and the study of the pressure dependence of the sulphur dioxide spectrum (Paper IV), shown in Fig. 4.2. Except for direct methods based on long path lengths, there are other related techniques, such as cavity ring down spectroscopy [95], capable of increasing the effective sample optical path length up to kilometres, in absorption cells of typical physical length of 0.3 to 1 m. Another technique for signal enhancement, which is suitable for low-power pump laser applications, is photoacoustic spectroscopy [96].

The light intensity used in the absorption measurement is also influencing the detected SNR. Generally, high radiation intensity will help to overcome both environmental and intrinsic noise, but particular care should be taken not to saturate the transition under investigation. Thus, if available, a high-power diode laser source will be preferable to use. Another aspect that influences the sensitivity is the quantum efficiency of the detector.

A brief overview of the noise sources applicable to the present work is given in Section 5.1. The basic aspects of frequency modulation and available sensitivities are discussed in Section 5.2, and long-path-absorption implementations are considered in Section 5.3.

5.1 Sources of Noise

Noise constitutes all unwanted signals that appear at the output of the detection system. The noise can be caused by external environmental sources or may be related to intrinsic properties of the measurement system. While environmental noise sources usually are easily identified and can to a large extent be eliminated, the intrinsic noise is a fundamental part of the instrumentation used and ultimately limits the detection.

Examples of environmental-noise sources frequently encountered are mechanical vibrations of the system optical components and atmospheric turbulence that cause fluctuations in the detected light intensity, and temperature drifts that influence wavelength stability. Some of the counter-measures, as discussed in Section 4.4, are fast sweep integration and line locking. Since environmental noise normally occurs at low frequencies, e.g., around 0.1-10 Hz for atmospheric turbulence, fast wavelength scanning up to kHz rates followed by signal averaging effectively reduces detection noise. Another environmental noise source, present especially outside well-controlled laboratory environments, is the fluctuating background radiation originating from the sun, road lights, lamps, etc. Their influence can be suppressed by employing narrow

interference filters or broader color filters, or time-gated detection. Absorption by other species and light scattering (causing spectral interferences and light attenuation) can be considered as external sources of noise that reduce the detection sensitivity.

The inherent noise factors of a diode laser spectrometer are due to the source, the detector, or the interaction between light and the optical system. The intrinsic fundamental noise sources and their origins are summarized briefly below:

- *Thermal (or Johnson) noise* originates from the random fluctuations of charge carriers in the detector electronics. It is independent of the incident power, and has a "white" noise spectrum, i.e. it does not depend on the frequency.

- *Shot noise* originates from the quantum nature of light. It depends on the incident power, but is independent of frequency.

- *Flicker (1/f) noise* is due to intrinsic laser properties (*laser excess noise)* and external noise sources. Intrinsic noise sources are photon and carrier density fluctuations, index of refraction variations, and partition noise (mode competition). External noise sources are, e.g., injection-current noise, temperature instabilities and background radiation changes. The noise spectrum has an approximate $1/f$ dependence, which is the main motivation for adopting high-frequency modulation schemes (see Section 5.2). The flicker noise is normally negligible at detection frequencies larger than a few MHz.

- *RAM-induced noise*. Frequency modulation is always accompanied by residual amplitude modulation (see Section 5.2), which manifests itself as an asymmetry at all the harmonics, and an offset in the first harmonic signal. The effect of this noise source can be seen as a slight asymmetry of the modulated signals in Papers I and VII.

- *Interference fringes* are an annoying source of noise, which frequently constitutes the limiting factor when using modulation techniques. The minimum detectable absorbance in the presence of interference fringes is in practice often set to $\sim 10^{-6}$. Diode lasers are particularly susceptible to optical feedback, as outlined in Section 3.3, and this can be induced by spurious reflection and scattering in the optical system. These accidental Fabry-Pérot fringes manifest themselves as an oscillating intensity background that can easily obscure weak absorption signals. The phenomenon is illustrated in Fig. 5.1, which is a recording of the direct absorption signals of sulfur dioxide around 302 nm overlapped with unwanted etalon fringes from internal reflections. Careful angling of all transmissive optics, use of reflective optics and wedged windows, dithering of optical components [97], and filtering techniques [98], are examples of methods used for fringe reduction.

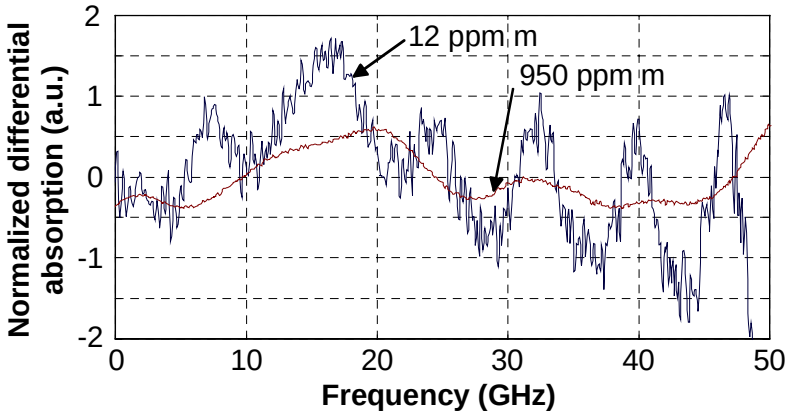

Fig. 5.1 *Direct absorption signals of sulfur dioxide (302 nm) at atmospheric pressure and with two different gas concentrations. The absorption at the lower concentration is totally obscured by unwanted interference fringes. According to the free spectral range of the interference fringes ($\Delta\nu_{FSR} \approx 8$ GHz), they were generated by an etalon cavity of approximately 20-cm length.*

5.2 Frequency Modulation

Detection of minute amounts of trace gases in the atmosphere by conventional direct absorption measurements frequently means that small intensity changes in large background signals have to be resolved. In order to improve detection sensitivity and to effectively discriminate against background noise, some kind of modulation technique can be employed. The fundamental concept of all modulation techniques is to shift the detection band to higher frequencies, where the noise level is small (see flicker noise in the previous section). This procedure also enables effective attenuation of low-frequency components by conventional filtering.

As discussed in Section 3.1.3, diode lasers can easily be modulated to frequencies in the kHz and MHz regime by changing the injection current. Depending on the frequency range, different types of frequency modulation techniques can be implemented. It should be mentioned that another option is to mechanically chop the laser beam at low frequency (a few kHz) and to detect the amplitude modulation (AM) signal phase sensitively using a lock-in amplifier. Absolute calibration and absorbance sensitivities of the order of 10^{-3} can be achieved using AM techniques.

In practice, frequency modulation is accomplished by superimposing a high-frequency sine wave on the wavelength-tuning ramping current. Since amplitude modulation always accompanies frequency modulation (see Section 3.1.3), the electrical field of the laser output radiation can be expressed as

$$E(t) = E_0\left[1 + M\cos\left(\omega_m t + \psi\right)\right]\sin\left[\omega_c t + \beta\cos(\omega_m t)\right]. \tag{5.1}$$

Here $\omega_c = 2\pi c/\lambda$ is the laser carrier frequency, ω_m is the modulation frequency, M is the AM index, ψ is the AM-FM phase shift, and β is the FM index defined according to

$$\beta = \frac{\Delta\nu}{\nu_m}, \tag{5.2}$$

where $\Delta\nu$ is the amplitude of the modulated signal. Thus, the FM index relates the maximum frequency deviation to the modulation frequency. The first term of Eq. (5.1) accounts for the amplitude modulation, while the second term is related to the frequency modulation. By expanding the AM term using Eulerian formulae and replacing the FM term by a summation over Bessel functions $J_p(\beta)$, Eq. (5.1) becomes

$$E(t) = E_0\sum_{p=-\infty}^{\infty} r_p(\beta, M, \psi)\exp\left(\omega_c t + p\omega_m t\right), \tag{5.3}$$

where r_p is defined as

$$r_p(\beta, M, \psi) \equiv J_p(\beta) + \frac{M}{2i}\left[\exp(i\psi)J_{p-1}(\beta) - \exp(-i\psi)J_{p+1}(\beta)\right]. \tag{5.4}$$

Equation (5.3), describing the laser electric field, shows that sine-wave modulation of the diode laser has the effect of generating multiple sidebands, as illustrated in Fig. 5.2(a). Each sideband is displaced from the carrier by an integer multiple (p) of the modulation frequency ω_m, with corresponding p:s opposite in phase. For pure frequency modulation ($M = 0$), the relative intensity of the sidebands depends on the FM index β. In the general case, however, the intensities in the upper and lower sidebands with equal p differ in magnitude due to superposition of AM and FM signals. This asymmetry leads to RAM-induced noise (see Section 5.1).

If no molecular absorption is present, the sidebands add up coherently with the carrier and there is a cancellation of the beat notes between them. When the laser field is scanned across an absorption feature of a gas, as shown in Fig. 5.2(a), the balance is lost and beat signals appear (for all multiple harmonics of ω_m). The strength of the absorption is proportional to the magnitude of the signal, which can be detected using frequency- and phase-sensitive electronics, e.g., a lock-in amplifier or a mixer. Consequently, frequency modulation can be used to determine gas concentrations, but an absolute calibration is needed. A typical FM setup for diode laser absorption spectroscopy is shown in Fig. 5.2(b).

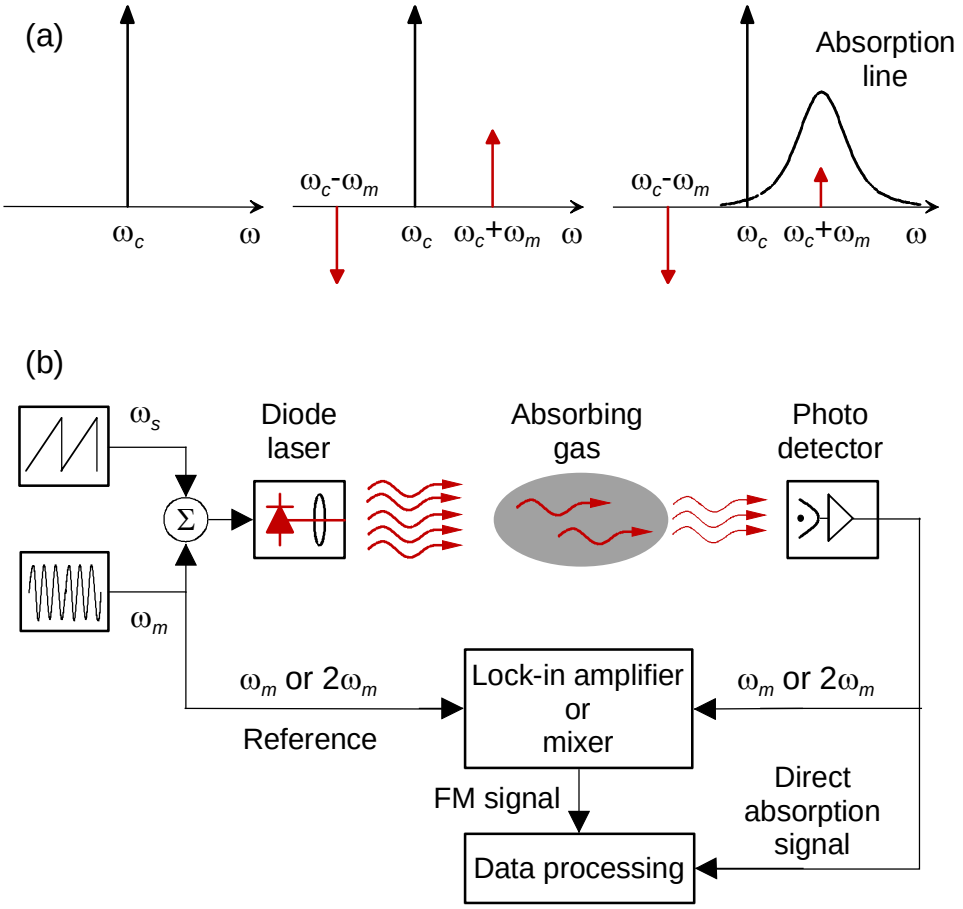

Fig. 5.2 *(a) Sideband generation around the laser carrier frequency (ω_c) by fast modulation (ω_m) of a diode laser. Scanning the laser wavelength at a low repetition rate (ω_s) across an absorption feature of a gas induces an imbalance when only one of the sidebands gets absorbed. (b) Schematic of a frequency modulation setup used for diode laser absorption spectroscopy of gaseous species.*

Depending on the magnitude of the modulating frequency ω_m, the FM techniques are divided into two categories: wavelength-modulation spectroscopy (WMS) [99], and frequency-modulation spectroscopy (FMS) [100]. The differences between these two modulation approaches are slight and partly semantic. By convention, WMS makes use of modulation frequencies ω_m that are much smaller than the halfwidth of the absorption line, and the modulation indices M and β are both large. The sidebands are present to a very high order and merge into a continuous spectrum. By contrast, FMS uses a modulation frequency comparable to or larger than

the halfwidth of the absorption line, and M and β are both small, so only the two first-order sidebands have appreciable magnitude. The theoretical descriptions of these methods, based on an intensity representation (WMS) and on an electric field approach (FMS), respectively, have strongly different formalisms [101].

WMS, also called *derivative spectroscopy*, usually employs modulation frequencies in the 1-100 kHz range, sometimes up to 1-10 MHz. The frequency and phase-sensitive detection can be performed either at the fundamental frequency ($1f$) or at some higher harmonic. Although the maximum signal amplitude is obtained for $1f$-harmonic detection, RAM of the diode laser can result in a large offset and limit the sensitivity. To reduce this offset and maximize the signal at the line center, the detection is most frequently performed at the second harmonic ($2f$). Generally, the signal at the n^{th} harmonic of the modulation frequency is similar with the n^{th} derivative of the absorption line. The signal is a true derivative only if the modulation amplitude is much smaller than the absorption line width, but under these conditions the signal is relatively small. Much larger signals are obtained with larger modulation amplitudes, which, however, distort and broaden the signal. To illustrate the high sensitivity obtained by modulation techniques, Fig. 5.3 shows two oxygen absorption spectra recorded using direct detection of the transmitted intensity and WMS, respectively. The large difference in SNR between the two recordings demonstrates the effectiveness of the method. Wavelength-modulation spectroscopy relies on relative low speed detectors, and the sensitivity is primarily limited by the flicker noise. The technique is particularly well suited for the study of atmospheric pressure-broadened and overlapping absorption lines that can extend over several gigahertz (see Chapter 4). WMS has been employed in the studies presented in Papers I, III, and VI-IX.

Frequency-modulation spectroscopy uses much higher modulation frequencies than normally employed in WMS, typically in the radio-frequency region (0.1-3 GHz). Only discrete components can be used in the detection electronics, essentially a phase-shifter and a mixer. Since radio-frequency components are small, FMS allows building smaller, lighter, and less expensive systems than WMS. The main advantage with the large modulation frequencies is that it maximises the differential absorption experienced by the sidebands, and that the laser excess noise is negligible at these frequencies (see Section 5.1). The major drawback is that relatively high-speed and, hence, expensive photo-detectors and detection electronics are required.

A variety of FMS, called two-tone frequency-modulation spectroscopy (TTFMS) [102], circumvents the use of high-speed detectors and electronics by using a heterodyne detection scheme. In TTFMS large modulation frequencies can be applied to maximise the differential absorption experienced by the sidebands. but detection is performed at a lower beat frequency (typically a few MHz), allowing the use of inexpensive low-bandwidth detectors. TTFMS has been employed in the studies presented in Papers I and II.

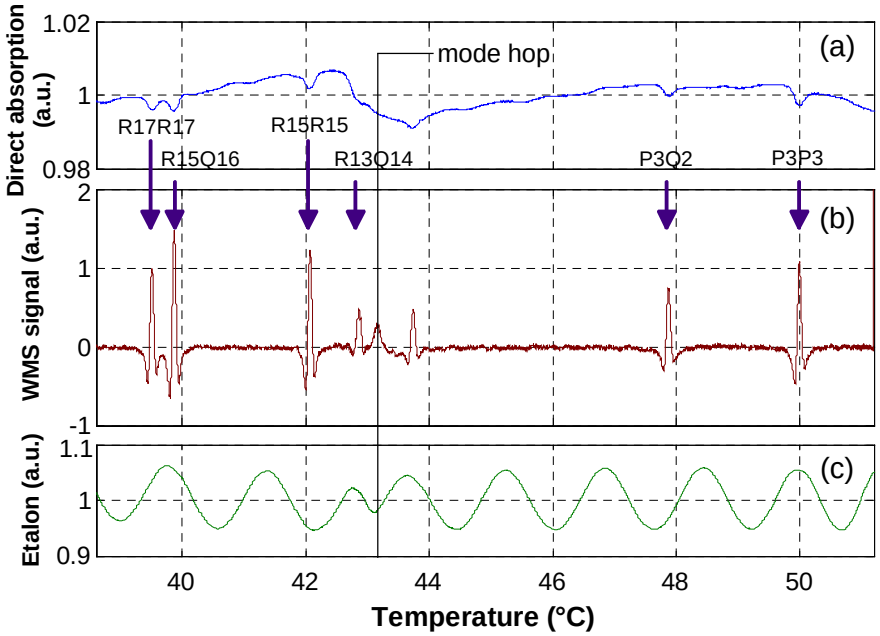

Fig. 5.3 *Simultaneously recorded (a) direct absorption and (b) WMS spectra of oxygen around 760 nm measured over a pathlength of 0.5 m in air. The etalon signal (c) provides the frequency scale. A mode jump, clearly visible as a discontinuity in the etalon pattern, is marked in the figure. The arrows indicate different lines belonging to the oxygen A band.*

Frequency modulation presents some important advantages that are common for both FMS and WMS. Owing to the derivative nature of the detection, FM is advantageous for the detection of sharp gas signals, as it discriminates against broad featureless absorptions, such as those from large organic molecules, or, as it will be presented in Section 6.2, from solid porous bulk material which contains gas. This aspect is important also in atmospheric trace gas detection, where weak absorption due to the wings of atmospheric pressure-broadened lines (e.g., H_2O) might cause systematic errors in direct absorption measurements. Another advantage is the absence of a large and sometimes sloping intensity background in the FM signals. However, the recorded spectrum does not provide any absolute calibration, which constitutes a drawback. Owing to this, a separate signal calibration has to be made (see Section 4.4).

Several scientific papers compare the sensitivity of the different frequency modulation techniques [103,104], but the results are not entirely consistent. The particular experimental arrangement used seems to influence the sensitivity for any particular modulation scheme. The best reported minimum detectable absorptions, specified for a signal-to-noise ratio (SNR) of 1 and a detection bandwidth of 1 Hz, are of the order of 10^{-7}-10^{-8} in FMS [105], and in the range of 10^{-5}-10^{-7} in WMS [104],

close to shot-noise-limited detection. In real applications, the sensitivity is often reduced to about 10^{-6} by the presence of interference fringes (see Section 5.1). Noise aspects and detection limits in FM are discussed in detail in Paper I and in Refs [106].

5.3 Long Path Absorption

There are two fundamental methods to achieve long optical path lengths in atmospheric sensing; either using a point monitor usually implemented by employing a multi-pass cell; or using a path-averaging line-of-sight arrangement, which frequently employs a double-pass system with a retroreflector. The method of choice depends on the specific application and the required parameter.

Two basic multipass cell designs are most commonly used in TDLAS instruments: the White and the Herriot cells. The laser beam is reflected multiple times, sometimes up to hundred times, and the effective sample optical path obtained for a physical length of the cell of 0.3-1 m can be more than 100 m. A variation of the Herriot cell uses astigmatic mirrors to achieve a longer path length for a given sampling volume (low volume means fast response) [107]. An advantage of using multipass cells is that the limitations of pressure broadening can be overcome by lowering the pressure either artificially or by using the cells on balloons at altitudes between 10-40 km.

The line-of-sight scheme can be used for remote sensing applications where the integrated value of the atmospheric trace gas concentration is of interest, e.g., in urban air quality monitoring. Although line-of-sight absorption measurements generally do not provide spatial information due to its incremental absorption nature, spatially resolved measurements can be achieved by combining multi-angular absorption spectroscopy with tomographic reconstruction techniques. Long-path measurements can conveniently be implemented by use of a retroreflector-telescope arrangement, as shown in Paper II. Two advantages are that the light traverses the optical path length twice, and that the setup is self-aligning up to a certain degree.

An advantage of free atmospheric monitoring is the absence of walls, gas extraction pipes, etc., which makes the arrangements insensitive to sampling. In most applications interference fringes are not present, but atmospheric turbulence can constitute a problem. The fast sweep integration method described earlier can be used to overcome the effects of turbulence on the detection. Another issue that should be considered, especially in urban environments, is laser safety. Preferably, eye-safe UV (<400 nm) or infrared radiation (>1.4 μm) should be employed in free atmospheric measurements.

For all long path absorption configurations, there is a limit for the sensitivity gained by extending the path length, due to increased loss in intensity that reduces the SNR at the detector. For example, a multipass cell with 98% mirror reflectivity and 100 single passes will exhibit a throughput of only 13%.

CHAPTER 6

LIGHT SCATTERING APPLICATIONS

Light scattering is one of the most prevalent phenomena in nature. The diffuse sun light scattered by the sky is lighting up our days, and the aura around a hazy moon is charming our nights; the white clouds and the colorful rainbow, are all due to light scattering by particles.

In the present work, light scattering has been used for aerosol particle identification by recording a Fourier transformed diffraction image. Light scattering in diffuse porous media is used in conjection with absorption spectroscopy measurements for analysis of embedded gas properties, such as concentration, pressure, diffusion properties; and for material characterization, e.g., scattering and absorption properties, porosity, and anisotropy.

6.1 Light Scattering

If light is impinging upon a particle – be it a molecule, an aggregate of molecules or an aerosol – part of the incoming wave will be scattered in different directions. This is due to emission of radiation from the electric charges in the particle, which have been accelerated by the electric field. The scattering is called *elastic* if the incident and scattered radiation have the same frequency, or *inelastic* if the wavelength is shifted by an amount corresponding to vibrational or rotational splittings in the energy structure of the molecule. Rayleigh and Mie scattering, as well as resonance radiation emitted upon absorption, are elastic scattering processes, while Raman scattering is inelastic. The Raman shift is characteristic for the molecule under study. The different scattering processes are illustrated schematically in Fig. 1.1.

There are two limiting cases for the phenomenon of elastic light scattering by small particles. If the particles are much smaller than the wavelength of light, *Rayleigh* (or *dipole*) *scattering* will distribute the scattered light homogeneously and symmetrically around the particle. In the case of *Mie scattering*, that pertains if the particles are comparable or greater in size than the wavelength of the impinging radiation, the scattered light is characterized by intensity oscillations in the scattering

directions [108]. Additionally, the scattered light intensity is strongly dependent of the particle size. In the case of Rayleigh scattering, the scattered light intensity is proportional to the sixth power of the particle diameter ($I \propto d^6$), while for Mie scattering, it is proportional to the particle's projected area ($I \propto d^2$). The scattered intensity increases towards shorter wavelengths with an approximate dependence $I \propto \lambda^{-4}$ for Rayleigh scattering, and $I \propto \lambda^{-2}$ for Mie scattering. In the atmosphere, Mie scattering from aerosol particles is normally more important than Rayleigh scattering from molecules. The visibility is determined by Mie scattering, and it would be hundreds of kilometers in the absence of scattering particles.

A detailed presentation of the theory of radiation and scattering processes can be found in [109].

6.1.1 Mie Scattering

As early as 1908, Gustav Mie presented an analytical method, based on Maxwell's equations of electromagnetic propagation, for derivation of the intensity distribution of light scattered by homogeneous spherical particles illuminated by a plane wave. In this section, aspects related to the present work, especially the development of an aerosol sensor [Paper V], are discussed. An extensive and detailed presentation of the complex Mie theory can be found in Ref. [108].

A parallel electromagnetic beam illuminating a particle is attenuated due to absorption and scattering by the particle. This attenuation of light, called extinction, can consequently be written as

Extinction = Scattering + Absorption.

At any point in the distant field, the scattered electromagnetic radiation has the character of a spherical wave, in which energy flows outward from the particle. The intensity distribution of the scattered light I_s, defined as energy flux per unit area, in a point at a distance r from the particle and corresponding to a scattering angle θ is given by

$$I_s(\theta, r) = \frac{Q_s(\theta, \alpha, m)}{k^2 r^2} I_0 , \tag{6.1}$$

where α is a dimensionless size parameter ($\alpha \equiv \pi d / \lambda$) interconnecting the particle size d and the radiation wavelength λ; Q_s is a dimensionless scattering function depending on the scattering angle θ, the size parameter α, and the complex refractive index m of the material ($m = n - ik$); k represents the wave number ($k = 2\pi / \lambda$), and I_0 is the illumination intensity. Figure 6.1 illustrates the strong angle dependence of the scattered intensity. It can be noticed that the lobe scattered in the forward

direction (0-20°) dominates, and that the forward-scattered light (0°) is 1-3 orders of magnitude larger than light scattered in other directions.

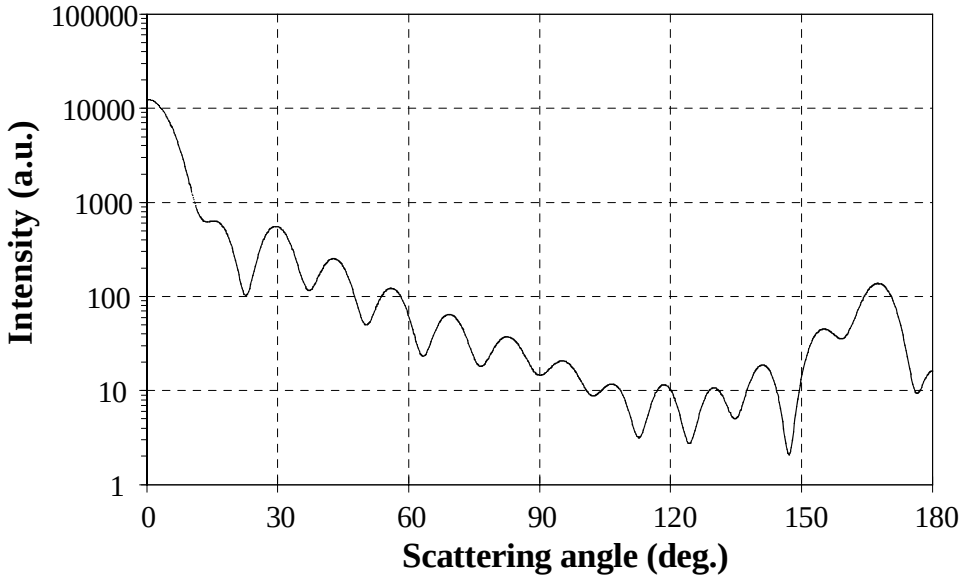

Fig. 6.1 *Scattered light intensity distribution due to electromagnetic radiation (λ = 780 nm) impinging on a spherical particle (α = 15, n = 1.5) in air.*

A scattering cross-section C_s, defined as the product of the scattering function Q_s and the cross-sectional area of the particle A_p, provides a measure for the amount of light scattered away from a beam by the particle. The light intensity absorbed inside a particle is defined as the energy incident on the area C_a, called the absorption cross-section. Thus, the total light intensity removed from the original beam corresponds to the so called extinction cross-section C_{ext}, defined as

$$C_{ext} = C_s + C_a . \tag{6.2}$$

It can be shown that for particles large compared to the wavelength of the incident light ($d \geq 4\lambda$), the extinction cross-section is equal to twice the cross-sectional area of the particle [109]. Similarly to the scattering cross-section C_s, an extinction cross-section C_{ext} can be defined as the product of an extinction efficiency factor Q_{ext} and the particle cross-sectional area A_p, i.e., $C_{ext} = Q_{ext} A_p$.

Geometrical optics can be employed for particles that are very large compared to the wavelength of light ($\alpha >> 1$). In the geometrical-optics limit it is useful to separate the scattering function into an independent and a dependent part with regard to the optical properties of the particle. The independent part can be approximated by Fraunhofer diffraction ($\theta < 10°$), while the dependent part describes scattering by reflection and refraction.

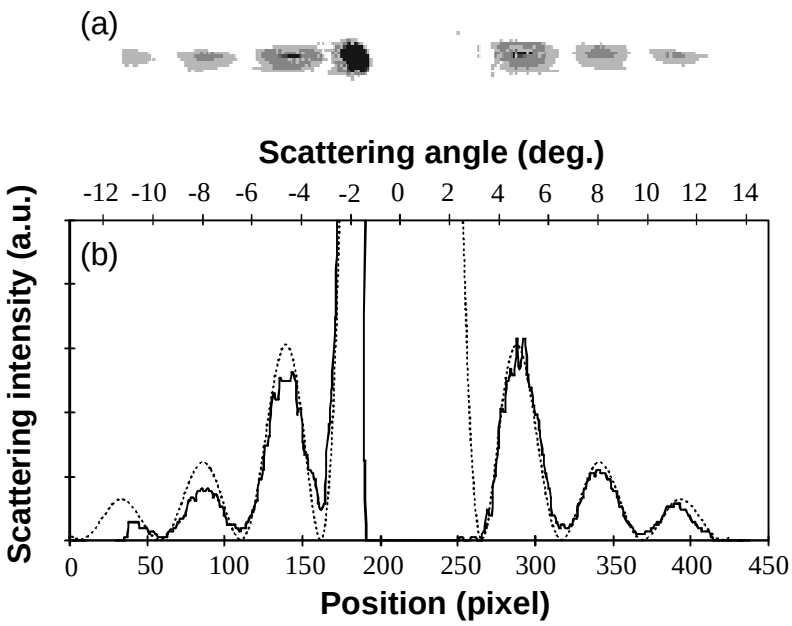

Fig. 6.2 (a) *Diffraction pattern from a carbon fiber (∅ 14 μm) illuminated with a laser beam (λ = 780 nm). (b) Cross-section of the diffraction image with a fitted Fraunhofer distribution (dashed line).*

In Paper V, the near-forward scattered light from single aerosol particles passing through the beam inside the coupled cavity of a diode laser, is imaged on a CCD camera for shape analysis and identification. The diffraction pattern is Fourier transformed by inserting the particles along the focal plane of an imaging lens. Thus, the diffraction pattern imaged by the lens is not influenced by the movement of the particles across the laser beam. An experimental recording of the diffraction pattern from a carbon fiber passing through the sensing volume of the detector is shown in Fig. 6.2(a). The thickness of the fiber was evaluated using a fitted Fraunhofer distribution, as shown by the dashed line in Fig. 6.2(b). The angular dependence of the diffraction minima for the fiber is the same as for a complementary slit, according to Babinet's principle, that is

$$d \sin\theta_m = m\lambda \,, \tag{6.3}$$

where d is the thickness of the fiber, θ_m is the scattering angle corresponding to the m^{th} irradiance minimum, m is a whole number $m = \pm1, \pm2, \pm3,\ldots$, and λ is the wavelength of the incoming light.

6.1.2 Light Propagation in Diffuse Media

When light is impinging upon a domain of scattering medium, it will be partly reflected off the surface, depending on the angle of incidence and the index of refraction of the material. The light penetrating the diffuse medium can either be absorbed or scattered, which is a highly wavelength dependent process. In the red and infrared wavelength region the scattering dominates over absorption.

Light propagation in diffuse media can be described mathematically either by analytical theory, based directly on Maxwell's equations, or by transport theory. Although less mathematically rigorous, transport theory offers the practical means to treat even complex structured materials. It does not take into account the wave property of light, but rather describes the problem as a flow of photon power through the scattering medium. The energy balance in an infinitesimal volume element in the scattering material at a position in space **r** is expressed in terms of the radiance, $L(\mathbf{r},\mathbf{s},t)$ [$Wm^{-2}sr^{-1}$], which is the radiant power per unit area and unit solid angle in direction **s**. The transport equation yields

$$\frac{1}{v}\frac{\partial}{\partial t}L(\mathbf{r},\mathbf{s},t) = -\mathbf{s}\cdot\nabla L(\mathbf{r},\mathbf{s},t) - (\mu_a + \mu_s)L(\mathbf{r},\mathbf{s},t) + \mu_s \int_{4\pi} L(\mathbf{r},\mathbf{s}',t)\,p(\mathbf{s},\mathbf{s}')d\Omega' + Q(\mathbf{r},\mathbf{s},t)\,, \tag{6.4}$$

where v is the velocity of light in the scattering material, $v = c_0 / n$, c_0 is the light velocity in vacuum, and n is the index of refraction of the scattering material; the scattering and absorption coefficients μ_a and μ_s describe the probability of a scattering event per unit length; the phase function $p(\mathbf{s},\mathbf{s}')$ represents the probability of changing scattering direction from $\mathbf{s}'$ into **s** after the scattering event. The left-hand side of Eq. (6.4) corresponds to the change in number of photons at position **r**, travelling in direction **s** at time t. The first two terms on the right-hand side denote the loss of photons due to escape over the volume boundaries, scattering into other directions, or absorption. The third term describes the gain through photons that are scattered from other directions into direction s. The last term denotes gain due to a light source. It is assumed that all photons have the same energy and that all scattering is elastic.

The transport equation is difficult to solve analytically. In practice, the methods used are either numerical, such as Monte Carlo simulations of photon migration, or

analytical by expansion in spherical harmonics leading to the diffusion equation. In the present work, the diffusion approximation was applied to light transmittance through an infinite slab of scattering material (see Paper VII). Hence, a brief description of this method is given in Appendix B.

Light transport theory and different methods to solve the transport equation have been treated in detail in Ref. [110]. A major application is in connection with light propagation in living tissue, which has implications to, e.g., optical mammography, dosimetry for photodynamic therapy, and concentration determinations for tissue and blood constituents.

6.2 Gas in Scattering Media

In the present work, exploratory studies of free gas dispersed inside highly scattering porous media were performed. The new technique, entitled **ga**s in **s**cattering **m**edium **a**bsorption **s**pectroscopy, GASMAS, opens up new possibilities for characterization and diagnostics of embedded gases as well as scattering solids and turbid liquids. Information about, e.g., internal gas concentration, pressure and temperature, as well as bulk material structure and diffusion properties can be conveyed.

6.2.1 Spectroscopic Aspects

A key feature of the GASMAS technique is its ability to separate the absorption signal of the internal gas from that of the surrounding bulk material. Owing to the complex interaction between the atoms, solid-state materials and liquids exhibit broad features (seldom sharper than 10 nm) in optical absorption spectroscopy. In contrast, gas detection relies on the narrow absorptive features of the free-gas molecules, which is in the order of 10,000 times sharper than the slow wavelength dependence of the absorption and scattering cross-sections in solids and liquids. It is advantageous to employ the frequency modulation techniques, presented in Section 5.2, to sensitively pick up the tiny but narrow gas imprint and discriminate it from the large but broad bulk absorption.

The experimental procedures for *in situ* detection of embedded gas resemble those used in conventional TDLAS in open air. However, extensive multiple scattering of the photons inside the porous material, caused by inhomogeneities of the optical properties of the medium, prevent the straightforward application of the Beer-Lambert law, which requires the optical path length to be known. The effective optical path length is normally much longer than the geometrical dimensions of the illuminated material and light emerges diffusely. The first GASMAS recordings [Paper VI] established an equivalent mean path length, which is the distance traversed by light in air, yielding a detected signal of the same magnitude as that from the absorption of photons by gas embedded in the porous material.

6.2.2 Probing Porous Solids

A prerequisite of the new gas-sensing technique is that light can be transmitted through the bulk material without being substantially absorbed. Surprisingly, many materials that look opaque to our eyes and seem difficult to penetrate by light can be diagnosed with the GASMAS technique, given that proper wavelength range, detectors, and geometry are selected. For instance, materials containing liquid water, e.g., biological tissue, cannot be investigated at wavelength longer than 1.4 μm.

An interesting and not yet solved issue is how light actually propagates inside the heterogenious medium. Some GASMAS-type experiments have indicated that there might be substantial waveguiding of the scattered light, either through the gas enclosures or through the bulk material, due to Fresnel refraction between materials having different refractive indices.

Most organic substances, and many natural and man-made materials are porous and contain free gas distributed throughout their bulk matrix. For instance, clouds, snow, ice, wood, plants, fruits, foams, powders, and sintered materials can be considered. Porous solid-structured materials in general take advantage of comparative strength in relation to their leight-weight characteristics. In the present work, polystyrene foam was extensively used as a model scattering material, owing to its relative high homogeneity, strong scattering properties, and high gas content, i.e., factors that contribute to a strong gas signature. Polystyrene foam also has a great industrial and commercial importance since it is extensively used as an insulation and packaging material.

The gas contents in liquids is a more delicate question. We know that aquatic creatures depend for their survival on the dissolved oxygen in water. Most likely the gas cannot be considered as free, and it does not render any sharp GASMAS signal. However, when water warms up and the gas solubility is reduced, visible bubbles will appear. This is, for instance, an everyday observation in the bed-side glass of water, or when opening a sparkling drink and the pressure suddenly is lowered. Small particles immersed in the liquid can act as condensation nuclei for bubble formation. Thus, in turbid liquids both scattering and bubble formation are expected to increase.

Proof-of-principle experiments of the GASMAS type were, for convenience, performed on molecular oxygen. This gas is normally diffused from the ambient atmosphere into porous materials, and, additionally, oxygen is also an essential physiological gas. The comparatively weak lines belonging to the oxygen A band around 760 nm, shown in Fig. 6.3, were probed with a commercial diode laser. Due to the high concentration of oxygen in air (20.8%) the resulting absorbance was relatively large. Virtually any gas, having sharp absorption features in the spectral regions where light can be transmitted through the bulk material, could be considered. Some of the most interesting species to be investigated are the biologically important gases carbon dioxide and water vapour, which monitored simultaneously with oxygen inside living organic materials could be used to diagnose metabolic processes.

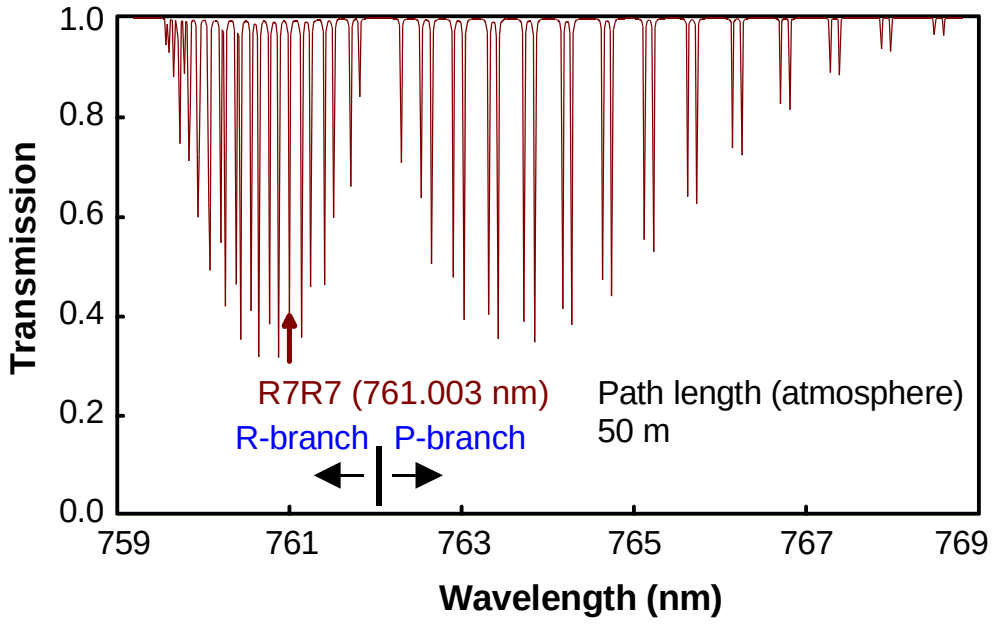

Fig. 6.3 *The oxygen A band. Marked with an arrow is the R7R7 line used in most of the GASMAS experiments.*

Two basic geometries can be considered when performing GASMAS-type measurements. In Fig. 6.4(a), a transillumination arrangement is presented, while in Fig. 6.4(b), a backscattering detection scheme is shown. In both cases, optical fibers can be used for both light injection and for collection of scattered radiation.

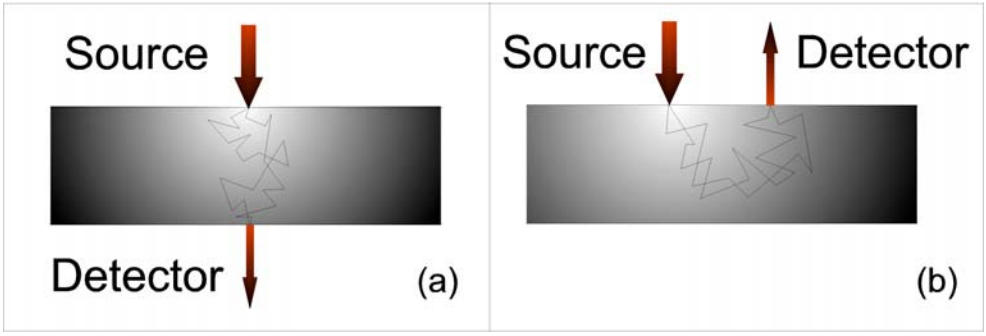

Fig. 6.4 *Basic geometrical arrangements for monitoring of free gas in scattering media: (a) transillumination, (b) backscattering.*

6.2.3 Detection in the Temporal Domain

To extract the concentration of gas embedded in a porous sample, additionally to the absorption measurement described previously, the powerful time-resolved measurement technique was utilized, employing a pulsed laser with an emitted wavelength close to the absorption line of the gas. The time-dispersion curves yield information on the "history" of the propagating photons, which have travelled different distances through the sample, as illustrated in Fig. 6.5. The figure shows an experimental curve obtained for a 40-mm-thick slab of oxygen-containing polystyrene foam, and indicates that some of the photons actually travel as far as 4 meters before reaching the detector. The successively stronger absorptive imprint in the light that has travelled longer distances is also schematically indicated. Figure 6.6 illustrates how the recorded pulse shape changes when light from a picosecond-pulsed diode laser is transmitted through differently thick slabs of polystyrene foam.

The analysis of the time-resolved data was based on the diffusion approximation to the radiative transfer theory (see Appendix B). In the case of transillumination through an infinite slab, the analytical relation for the transmitted light intensity is given by Eq. (B.12). Thus, the optical properties of a sample can be evaluated by fitting such an analytical expression to the experimentally acquired temporal dispersion curves by adjusting the free parameters; i.e., the absorption and the reduced scattering coefficients, μ_a and μ_s', respectively.

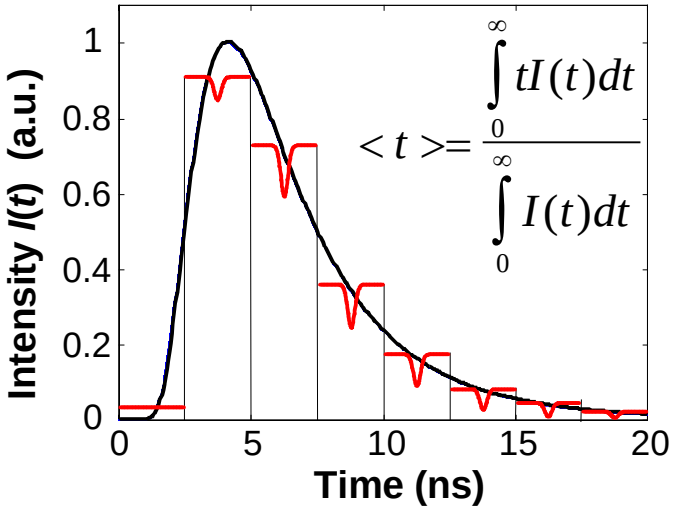

Fig. 6.5 *Schematic illustration of the contributions from differently long path lengths to the measured gas signal in the case of a 40-mm-thick slab of polystyrene foam.*

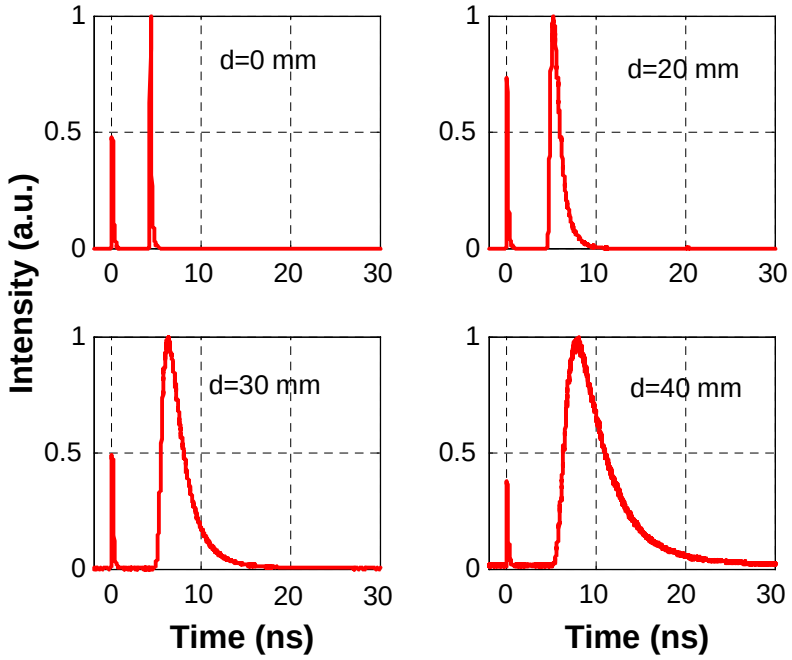

Fig. 6.6 *Time-dispersed curves of differently thick slabs of polystyrene foam measured by utilizing ultra-short light pulses from a diode laser tuned close to 760 nm.*

The average time-of-flight of the photons <*t*> can be evaluated by integration of Eq. (B.12), and is given in the general case by

$$\langle t \rangle = \frac{\int_0^\infty tI(\mathbf{r},t)}{\int_0^\infty I(\mathbf{r},t)}, \tag{6.5}$$

where $I(\mathbf{r},t)$ denotes the emerging diffuse light intensity on the boundary of the sample at a point **r** and time *t*. The average travel time yields the mean absorption path length. Thus, the concentration of the embedded gas can be assessed by using the Beer-Lambert law, as demonstrated in Paper VII. For an infinite slab of thickness *d*, it has been found that in the case of weak absorption and strong scattering properties, the average time-of-flight – related to the equivalent mean path length – is proportional to the square of the thickness of the slab, i.e. $< t > \propto d^2$. A similar relationship was also obtained considering the related topic of light propagation through clouds [111], where the weak A-band lines of oxygen become more absorbed.

6.2.4 Applications of GASMAS

A particularly interesting application of the GASMAS technique is the study of gas diffusion through porous materials. It has been realized by initially storing the sample in a nitrogen atmosphere for a few hours, and subsequently taking it out and placing it in the GASMAS apparatus, where the successive re-invasion of ambient air into the sample can be followed by the oxygen signal, as shown in Fig. 6.7. Here a 10-mm-thick samples of Norwegian Spruce and Balsa wood were studied, and, contrary to what could have been expected, the Balsa wood exhibits a much longer time constant, probably related to sealed individual cell compartments in the otherwise loose fibrous matrix. This demonstrates that diffusion can be characterized by several time constants.

In Paper VIII the gas diffusion in wood of different kinds is studied. Gas exchange in building and construction materials is clearly of substantial interest for a large industrial sector, in view of moisture problems and release of unwanted agents ("sick houses"). The influence of surface coatings such as paints or plastic films can also be readily studied [112].

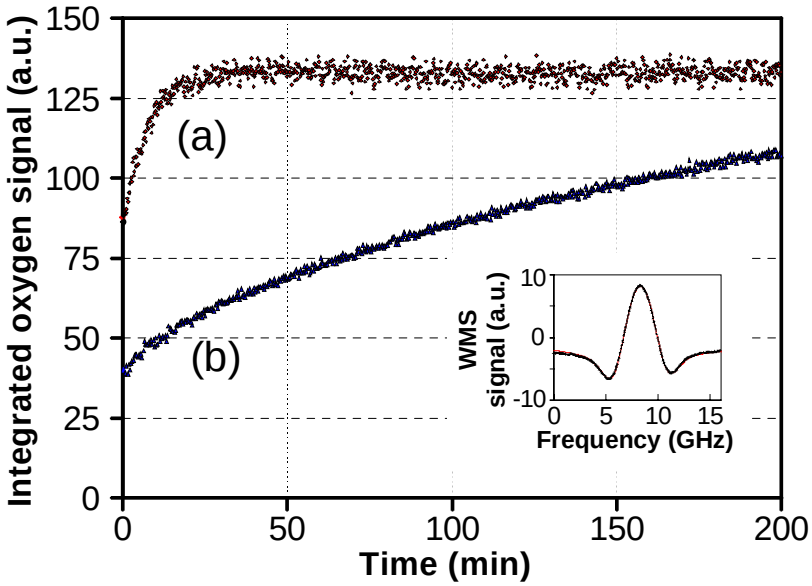

Fig. 6.7 *Re-invasion of atmospheric oxygen into two 10-mm-thick slabs of (a) Norway Spruce and of (b) Balsa, respectively. A typical detected modulation signal is shown in the insert.*

By use of these techniques it would be possible to monitor *in situ* physiological and degradation processes in various biological substances. Such measurements have

been limited to extraction of emitted gas from, e.g., plants, fruits, and insects, measured by normal gas spectroscopic techniques. The largest challenge would be to develop methods for monitoring minute amounts of free gas inside human tissue, possibly allowing development of new diagnostic techniques for diseases.

In the preservation of foodstuffs it is important to keep atmospheric oxygen away, which is frequently accomplished by use of plastic films or laminates [112]. This is the case for, e.g., meats packaging, where the films also have the additional purpose of preventing drying out and bacterial access. Related techniques are used for beverages, especially milk. It can be anticipated that the GASMAS technique can have important applications also in these contexts.

Monitoring of concentration ratios of gases absorbing at close-lying wavelengths eliminates the need for a detailed understanding of the photon transport through the sample and could give new insights in fields as diverse as plant physiology and catalyst research.

CHAPTER 7

GAS CORRELATION SPECTROSCOPY

The underlying principle of gas correlation spectroscopy can simply be stated as "nobody knows a molecular absorption spectrum better than the gas itself", i.e., the gas can be used as its own spectral filter for identification and quantification purposes. In this chapter the gas correlation technique will be briefly described, and its application to diode laser absorption spectroscopy is presented.

7.1 Using Broadband Sources

Gas correlation spectroscopy, also known as the gas filter correlation spectrometer (GASPEC) [113], has been in use for many years. Already in 1943 K. Luft described an early version of this device [114].

The basic idea of the correlation spectroscopy approach is particularly simple and powerful. It involves a comparison between the absorption spectrum of a target gas of interest contained in a reference cell, and an external gas to be measured. The purpose is to identify the presence and estimate the concentration of the target gas in the unknown external gas mixture.

Broadband radiation which has been passed through the external gas mixture is either sent directly to a detector or is additionally filtered through a reference cell containing an optically thick amount of the target gas. Thus, the incoming light is selectively filtered by being absorbed in the reference cell at specific wavelengths corresponding to the gas signature, but it is readily transmitted through the sample optical path. Thus, the wavelength-integrated light intensity passing through the reference cell is largely independent of the presence of the target gas in the external mixture, whereas the light intensity detected directly is strongly dependent upon the presence of the target gas. Hence, the difference in spectral transmittance between the two paths is a sensitive indicator of the presence and the amount of the target gas in the external mixture.

A particularly powerful application of the gas correlation technique to gas imaging has been developed [115,116]. The method utilizes the thermal background

for detection of gas absorption or emission in the infrared wavelength region, and allows for visualization and quantification of gas flows.

7.2 Using Diode Lasers

A novel application of the gas correlation technique has been proposed and demonstrated in Paper IX. The main concern of this gas analysis scheme, denoted temporal gas correlation spectroscopy, is to address some of the shortcomings of the TDLAS technique, namely its susceptibility to emission frequency instability, including mode competition and mode hops, thermal drift, and change of wavelength characteristics due to ageing. All these intrinsic properties of diode lasers frequently impair their applicability to gas spectroscopy. By combining the simplicity and robustness of the gas correlation technique with the high sensitivity and high resolution of the TDLAS, less stringent requirements on the diode lasers used in spectroscopic measurements are achieved. This should facilitate real-world implementation of diode laser spectrometers in a wide field of applications.

A schematic of the principles of the new technique is shown in Fig. 7.1. Similarly to gas correlation spectroscopy, the radiation is split into two beams. Thus, the narrow-band laser beam is being passed either through the external gas or through a reference cell containing the target gas, which in this case is not totally absorbing and can be utilized also for calibration purposes. When the diode laser is wavelength-tuned across absorption features of the gas of interest, light intensity variations due to mode

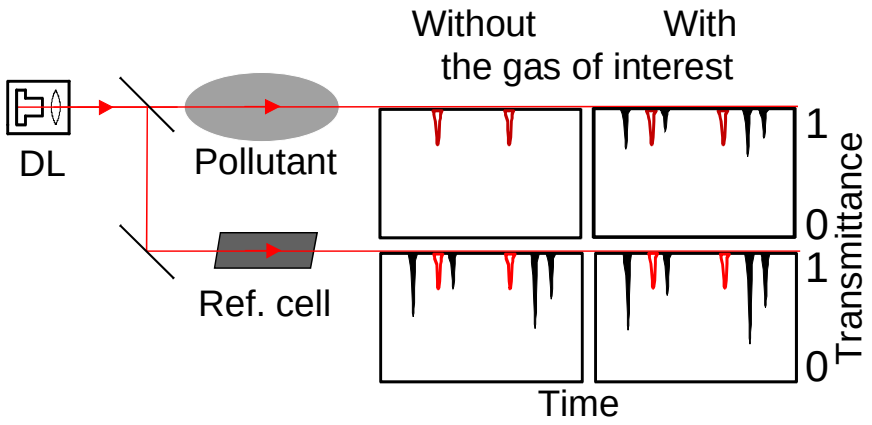

Fig. 7.1 *The principles of the temporal gas correlation spectroscopy scheme. The filled lines represent gas absorption features, while the empty lines correspond to intensity fluctuations related to diode laser mode hops.*

competition or mode hops are interfering with the gas absorption. By simultaneous recording of the external and the reference gas signals, as well as the laser output power during the scan, a correlation procedure described in Paper IX can be used to eliminate the unwanted influence of the mode instabilities. Because of the simultaneousness of the measurements even the effect of thermal drift is acounted for. Proof-of-principle measurements have been performed on atmospheric oxygen in both steady-state and dynamic gas diffusion experiments.

The temporal correlation spectroscopy scheme can in principle be applied to any gas with close lying and fairly sharp absorption features, and allows for the use of non-sophisticated multimode diode lasers, which are less expensive and offer higher output powers. Although the detection sensitivity is lower than for conventional TDLAS, the new technique could find applicability in fields where the major requirement is long-term reliable operation and minimum of maintainance.

ACKNOWLEDGEMENTS

I would like to express my sincere gratitude to my supervisor, Professor Sune Svanberg, who through his boundless enthusiasm and profound knowledge of physics has been a true inspirer in my research work. What impressed me the most, however, is Sune's personal warmth and considerate attitude, being always supportive, finding always the best solutions.

I also much enjoyed working together with my near collaborators and friends. I am very grateful to Ulf Gustafsson for his friendship and helpfulness, to Mikael Sjöholm for all discussions and nice joint work, to Janis Alnis for the pleasure of working together with an enthusiastic experimentalist, to Jonas Sandsten for his dedication and professionalism, and to Petter Weibring for all the fun we had together both at work and on the climbing wall.

The support from my collegues at the Atomic Physics Division cannot be overestimated. A special thank to Anders Persson, who can help to solve the most intricate technical problems without even noticing how difficult they are, to Hans Edner and Stefan Andersson-Engels for sharing their scientific knowledge, to Laila Lewin and Britt-Marie Hansson for giving a helping hand whenever a critical situation arises, to Åke Bergquist and Bertil Hermansson for making the perfect electronics and keeping computers alive.

My younger collegues in the Molecular Spectroscopy group, Linda Persson, Magnus Bengtsson, and Rasmus Grönlund, diserve my deepest gratitude for co-operation and for creating such a pleasant atmosphere.

Thanks also to all the foreign friends I got to know: to Zhang Zhiguo and Gao Hong for nice joint work in the lab and for teaching me Chinese technical terminology 谢谢!; to Benjamin Andersson, and to Manny Mathuthu and Louis Olumekor, who welcomed me so cordially while at University of Zimbabwe in Harare; to Jim Smith, Xu Huailiang, and César de la Costa.

Thanks to Joakim Nordqvist for the insights you shared with me about energy, climate and cement issues, and for a very rewarding research trip to China.

Thanks to my dear friends, Richard and family, Rita and Jörgen, Sheryl and Vikas – your good spirits and support sheded much joy in my heart.

I would like to thank my family for all their support and encouragement through the years. Especially to my mother, Teresia, for her boundless love and unyielding support. Köszönöm!

Finally, I would like to thank my wife, Lanlan, for her encouragement and love, and my daughters Alma and Emelie – the flowers in my life – for bringing so much joy to us.

SUMMARY OF PAPERS

Paper I High-sensitivity absorption measurements using frequency-modulation spectroscopy with blue continuous-wave diode lasers were demonstrated for ground state potassium atoms, and lead atoms in very weakly populated meta-stable states.

Paper II Traffic-generated emission of nitrogen dioxide was monitored *in situ* using long path absorption combined with two-tone frequency modulation spectroscopy. The possibility of using comparatively weak nitrogen dioxide absorption lines around 635 nm was pointed out.

Paper III The first published paper on laser spectroscopy employing blue continuous-wave diode lasers. High-resolution ultraviolet spectroscopy of mercury isotopes around 254 nm was performed by sum-frequency generation. Mercury detection at atmospheric pressure was demonstrated.

Paper IV A diode-laser-based spectrometer for high-resolution detection of sulfur dioxide is presented. Ultraviolet radiation around 300 nm was produced using a sum-frequency generation scheme employing a blue and a near-infrared diode laser. Pressure dependence studies of sulfur dioxide lineshapes were performed.

Paper V A new single aerosol particle detector using a coupled-cavity diode laser was developed. A distinguishing feature is the simultaneous size and shape determination by measurement of the optical extinction due to the particle, and the resulting diffraction image in the near-forward scattered light.

Paper VI-VIII In these papers, a novel technique for analysis of free **ga**s in **s**cattering **m**edia by use of **a**bsorption **s**pectroscopy, GASMAS, is introduced. The sharp absortive features of the gas, contrasted to the very slow wavelength dependence of the bulk material, can be picked up by use of modulation techniques. In *Paper VI* proof of principle measurements were performed on dispersed molecular oxygen embedded in various natural and man-made porous materials. Internal gas pressure and gas-exchange assessment were demonstrated.

In *Paper VII*, concentration measurement of gas embedded in scattering materia was accomplished by employing absorption and time-resolved laser spectroscopy. The mean path length of the scattered light was determined and found to be proportional to the square of the scattering medium thickness. In *Paper VIII*, application of the technique to the study of various wood samples is presented. Gas diffusion characteristics were investigated, and promising extensions to, e.g., gas adsorption in catalysts embedded in porous materials, were discussed.

Paper IX A new temporal correlation scheme was developed to address the intrinsic multimode and mode-hop behaviour of diode lasers, that often impair their spectroscopic applicability. An unknown concentration of the gas under study was determined by temperature tuning a diode laser across absorption features of the gas. The light intensity fluctuations due to mode-hops could be eliminated by simultaneous temporal correlation of the detected signal with the signal from a known reference gas concentration. No knowledge of the exact spectrum was needed. The method was tested in diffusion related measurements.

Contribution by the author to the papers

Paper I Contribution to system integration, experimental work, and manuscript preparation.

Paper II Major part of system integration, field measurements, analysis and manuscript preparation.

Paper III Involvement in experimental build-up, and contribution to the measurements.

Paper IV Responsible for experiment planning and system integration. Major part of experimental work and manuscript preparation. Contribution to data evaluation.

Paper V Major part of experimental work. Contribution to system construction and integration, theoretical modeling, data evaluation and manuscript preparation.

Paper VI Substantial part of system integration, measurements, data evaluation and manuscript preparation.

Paper VII Substantial part of system integration and measurements. Major part of manuscript preparation. Involvement in data evaluation.

Paper VIII Substantial part of system integration, measurements and manuscript preparation. Involvement in data evaluation.

Paper IX Responsible for system design and experiments, except for data acquisition. Major part of manuscript preparation. Involvement in data evaluation.

Appendix A

COUPLED-CAVITY MODEL

In Paper V a coupled-cavity diode laser arrangement is used to determine the equivalent size of an aerosol particle by means of the recorded extinction loss signal. Below a simple coupled-cavity model is described, which relates the particle cross-sectional area to the change in monitored output power. In the following, reference is made to Fig. A.1.

Using a single-reflection approximation, the coupled cavity is considered equivalent to a solitary diode laser with an effective reflectivity of the coupled facet R_e given by

$$R_e = R_2 + (1-R_2)^2 k R_{ext} = R_2 + (1-R_2)^2 R_3, \tag{A.1}$$

where R_1 and R_2 are the front and back facet reflectivities, respectively, of the solitary diode laser, R_{ext} is the external plane mirror reflectivity, and k ($0 \le k \le 1$) is a coupling coefficient accounting for reflection losses, as shown in Fig. A1(a).

If a particle is present in the radiation field inside the coupled cavity, part of the light is lost due to particle-induced scattering and absorption (see Section 6.1.1). The effective reflectivity of the coupled facet R_p becomes

$$R_p = R_2 + (1-R_2)^2 \left(1 - \frac{Q_{ext} A_p}{A_b}\right)^2 R_3, \tag{A.2}$$

where the additional factor $\left(1 - Q_{ext} A_p / A_b\right)^2$ accounts for the particle-induced extinction loss; Q_{ext} is the extinction efficiency factor, A_p is the cross-sectional area of the particle, and A_b is the equivalent "top hat" laser beam cross-sectional area inside the coupled cavity, as shown in Fig. A1(b).

The output power of the unperturbed coupled cavity P_e varies proportionally with the operating current I and can be expressed as [85]

$$P_e = \frac{\hbar\omega}{e}\left(I - I_{th,e}\right)\eta_i \frac{\ln\left(1/R_1\right)}{2\alpha_i L + \ln\left(1/R_1 R_e\right)}, \tag{A.3}$$

where $\hbar$ is Planck's constant, e is the electron charge, $I_{th.e}$ is the unperturbed threshold current, and the cavity parameters are: ω the radiation frequency of the diode, η_i the internal quantum efficiency to account for spontaneous emissions and leakage currents, α_i the intrinsic loss per unit length due to material absorption and scattering inside the laser diode cavity, and L the diode cavity length.

Analogously, with a particle perturbing the system, the output power P_p becomes

$$P_p = \frac{\hbar\omega}{e}\left(I - I_{th,p}\right)\eta_i \frac{\ln\left(1/R_1\right)}{2\alpha_i L + \ln\left(1/R_1 R_p\right)}, \tag{A.4}$$

where $I_{th,p}$ is the increased threshold current in the presence of a particle.

Assuming that the threshold current of the perturbed coupled cavity system varies linearly with the variable effective reflectivity yields

$$I - I_{th,p} = \left(I - I_{th,e}\right)\frac{R_p - R_2}{R_e - R_2}. \tag{A.5}$$

The particle-induced extinction loss S is defined as

$$S = \frac{P_e - P_p}{P_e} = 1 - \frac{P_p}{P_p}. \tag{A.6}$$

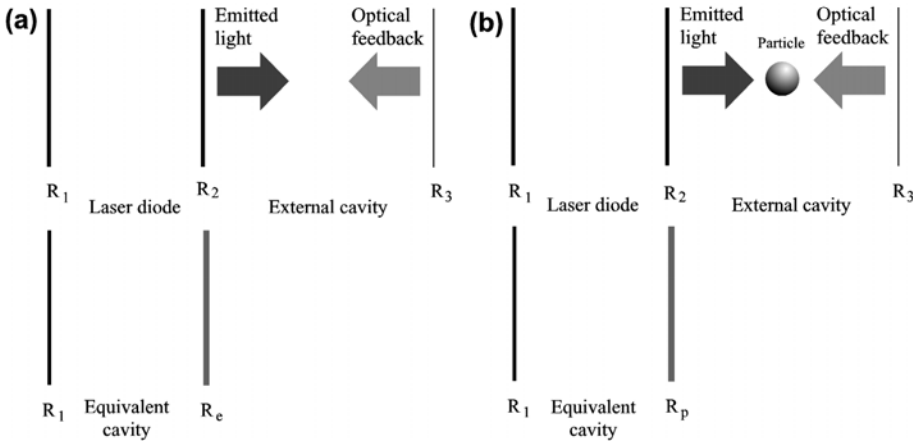

Fig. A.1 *Diagram of a one dimensional coupled-cavity diode laser: (a) with weak feedback from an external mirror, and equivalent solitary diode scheme; (b) with a small particle inside the external cavity, and equivalent scheme.*

Substituting Eqs (A.3-5) into this expression yields

$$S = 1 - \frac{P_p}{P_e} = 1 - \frac{\left(R_p - R_2\right)}{\left(R_e - R_2\right)} \frac{2\alpha_i L + \ln\left(1/\ R_1 R_e\right)}{2\alpha_i L + \ln\left(1/\ R_1 R_p\right)}. \tag{A.6}$$

By assuming that $A_p << A_b$, the perturbed reflectivity R_p can be related to the unperturbed reflectivity R_e yielding

$$R_p \approx R_2 + \left(1 - R_2\right)^2 R_3 \left(1 - 2\frac{Q_{ext} A_p}{A_b}\right) = R_e \left(1 - 2\frac{Q_{ext} A_p}{A_b}\left(1 - R_2\right)^2 \frac{R_3}{R_e}\right) = R_e\left(1 - y\right), \tag{A.7}$$

where y is a small number. Substituting this expression into Eq. (A.6) it is found that the particle-induced extinction loss can be approximated as

$$S \approx 2\frac{Q_{ext} A_p}{A_b} \approx 4\frac{A_p}{A_b}, \tag{A.7}$$

where the assumption was made that the particle size is larger than 4λ ($Q_{ext} \approx 2$).

In conclusion, the extinction loss due to small particles ($A_p << A_b$) inside the coupled cavity is approximately twice as large as if the particles were outside the laser cavity, i.e., $S = Q_{ext} A_p / A_b \approx 2A_p / A_b$.

Appendix B

THE DIFFUSION APPROXIMATION

The transport equation, given in Eq. (6.4), may be solved analytically by expanding the radiance $L(\mathbf{r},\mathbf{s},t)$, the phase function $p(\mathbf{s},\mathbf{s}')$ and the source function $Q(\mathbf{r},\mathbf{s},t)$ in spherical harmonics.

The radiant energy fluence rate $\varphi(\mathbf{r},t)$ [Wm^{-2}], defined as the radiant power incident on a small sphere divided by the cross-sectional area of the sphere, is introduced according to

$$\varphi(\mathbf{r},t) = \int_{4\pi} L(\mathbf{r},\mathbf{s},t)\,d\Omega\,. \tag{B.1}$$

Further, the photon flux vector $\mathbf{F}(\mathbf{r},t)$ [Wm^{-2}], which describes photon energy transfer per unit area, is given by

$$\mathbf{F}(\mathbf{r},t) = \int_{4\pi} L(\mathbf{r},\mathbf{s},t)\,\mathbf{s}\,d\Omega\,. \tag{B.2}$$

The lowest order (P_1) approximation to the transport equation includes only the zeroth and the first terms in the infinite series expansion. The radiance is then given by

$$L(\mathbf{r},\mathbf{s},t) \approx \frac{1}{4\pi}\varphi(\mathbf{r},t) + \frac{3}{4\pi}\mathbf{F}(\mathbf{r},\mathbf{s},t)\cdot\mathbf{s}\,. \tag{B.3}$$

The first term on the right-hand side of Eq. (B.3) corresponds to a totally isotropic light field, while the second term represents a small directional perturbation. The flux can be related to the fluence rate according to Fick's law

$$\mathbf{F} = -D\nabla\varphi\,. \tag{B.4}$$

The diffusion coefficient D is given by

$$D = \left[3\left(\mu_a + \mu_s'\right)\right]^{-1}, \tag{B.5}$$

where a reduced scattering coefficient μ_s' is introduced, defined as

$$\mu_s' = \mu_s(1-g). \tag{B.6}$$

Here the anisotropy factor g is the mean cosine of the scattering angle θ. The value of g is close to zero for nearly isotropic scattering, and close to unity for strongly forward directed scattering. Equation (B.6) describes a transform from non-isotropic to isotropic conditions, yielding a coefficient for the effective isotropic scattering.

The spherical harmonics of the radiance, phase function and source function can now be inserted into the transport equation, and by using Fick's law, this yields the diffusion equation

$$\frac{1}{v}\frac{\partial}{\partial t}\varphi(\mathbf{r},t) - D\,\Delta\varphi(\mathbf{r},t) + \mu_a\varphi(\mathbf{r},t) = S(\mathbf{r},t), \tag{B.7}$$

where $S(\mathbf{r},t)$ [Wm^{-3}]is a source term. It has been assumed that the scattering medium is homogeneous, hence the diffusion coefficient is constant. The diffusion approximation is only valid if the light distribution can be considered as diffuse. It means that the reduced scattering coefficient must be much larger than the absorption, i.e., $\mu_s' >> \mu_a$, and that the point $\mathbf{r}$, where we are looking, is far from sources and boundaries. The first requirement is true for most scattering media in the red and near-infrared wavelength region.

The diffusion equation can be solved analytically for some simple geometries, and the solution has to fulfill the boundary conditions. Since in the present work the transilluminated slab geometry was considered, solutions for this particular case will be given.

If a short light pulse from an isotropic source is sent into a turbid medium, the transport of photons will cause a temporal broadening of the pulse, as shown in Fig. B.1(a) for the case of transmittance. By measuring this broadening, it is possible to extract information about the optical properties of the material. Alternative measurement techniques to obtain these properties include frequency domain and spatially resolved steady-state measurements, also illustrated in Fig. B.1(b) and (c), respectively. Below, the mathematical tools to derive the optical properties from temporal and spatial resolved measurements will be presented.

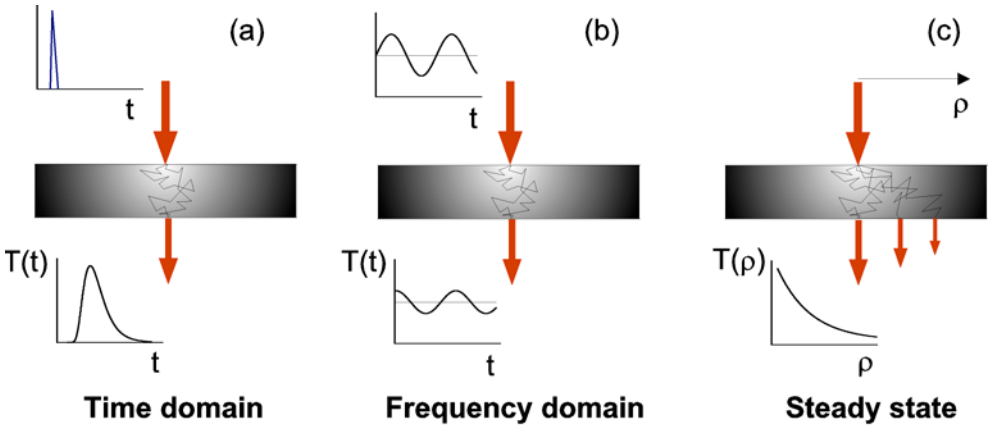

Fig. B.1 *Optical transmittance measurements performed in: (a) time domain, (b) frequency domain, (c) spatial domain (steady state measurements).*

The solution to the diffusion equation in an infinite medium for an isotropic point source described by a delta function, $S(\mathbf{r},t) = \delta(0,0)$, is given by the Green's function

$$\varphi(\mathbf{r},t) = v(4\pi Dvt)^{-3/2} \exp\left(-\mu_a vt - \frac{\mathbf{r}^2}{4Dvt}\right). \tag{B.8}$$

This function can be used to determine the fluence rate in other simple geometries, such as a homogeneous slab. In the case of a narrow beam of light incident upon the surface of a scattering media, the primary source term can be described as an isotropic point source at a depth equal to the mean free path of isotropic scattering,

$$z_0 = \left(\mu_s'\right)^{-1}. \tag{B.9}$$

Assuming that all incident photons are initially scattered at this depth will not yield any significant inaccuracies in fluence rates far from the source. The boundary conditions for the interference between the scattering medium and air must also be satisfied. The requirement is that the photon flux from the surrounding air back into the medium is zero. In the case of a slab with finite thickness and infinite expansion, the most common approach is to mirror an infinite set of imaginary positive and negative isotropic sources in both surfaces of the slab, as illustrated in Fig B.2. If Fresnel reflections at the surface are also taken into account, an extrapolated boundary at some distance beyond the actual surface has to be introduced, but the correction is small. The depth of the imaginary sources used to fulfill the boundary conditions is given by

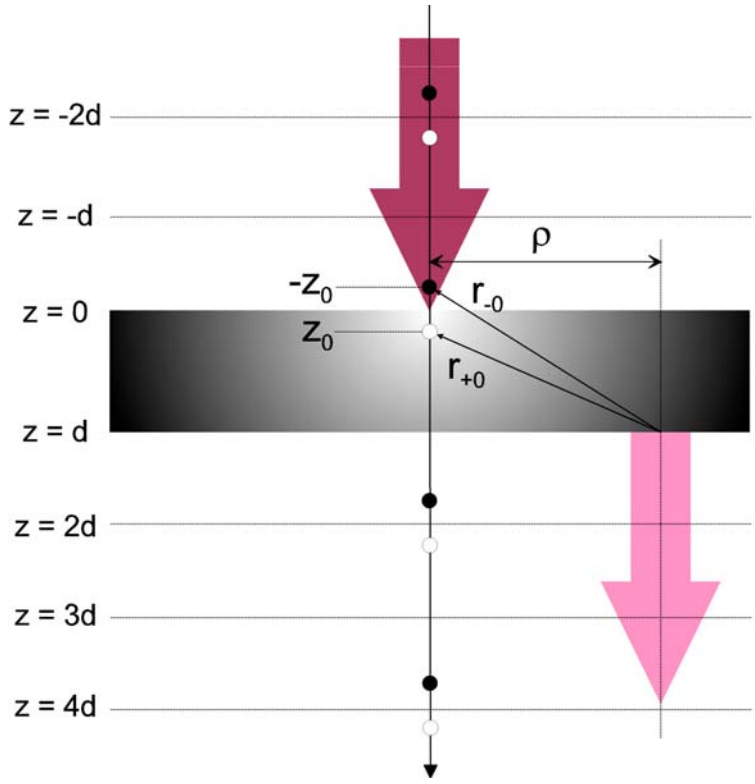

Fig. B.2 *Boundary condition for an infinite-slab geometry. Isotropic point source at a depth z_0 into the medium, and a set of imaginary positive and negative sources mirrored in both surfaces of the slab.*

$$z_{\pm k} = (2k+1)d \pm z_0 , \tag{B.10}$$

where d is the thickness of the slab, and k is a whole number k = 0, ±1, ±2,… Here z = 0 represents the slab boundary at the back surface. Thus, the corresponding distance between the detector position and the k^{th} source used in the calculations becomes

$$r_{\pm k} = \left(\rho^2 + z_{\pm k}{}^2\right)^{1/2}, \tag{B.11}$$

where ρ is the injection-detection separation.

Thus, the transmitted pulse shape can be described in terms of the absorption coefficient μ_a and the reduced scattering coefficient μ_s' of the sample material. The

analytic expression for the time-dependent transmitted intensity in the case of an infinitely extended slab of scattering material, can be expressed as

$$I(\rho,d,t) = (4\pi Dv)^{-3/2} t^{-5/2} \exp\left(-\mu_a vt - \frac{\rho^2}{4Dvt}\right)$$
$$\times \sum_{k=0}^{+\infty}\left[z_{-k} \exp\left(-\frac{r_{-k}{}^2}{4Dvt}\right) - z_{+k} \exp\left(-\frac{r_{+k}{}^2}{4Dvt}\right)\right]. \quad \text{(B.12)}$$

In the steady-state case, the diffusion equation Eq. (B.7) becomes

$$D\,\Delta\varphi(\mathbf{r}) + \mu_a \varphi(\mathbf{r}) = Q(\mathbf{r}), \quad \text{(B.13)}$$

where $Q(\mathbf{r})$ is a modified source term. The Green's function describing the fluence at a distance r from a point source at the origin in an infinite medium is

$$\varphi(r) = (4\pi Dr)^{-1} \exp\left(-\mu_{eff} r\right), \quad \text{(B.14)}$$

where μ_{eff} is the effective attenuation coefficient of the material, defined as

$$\mu_{eff} = \left[3\mu_a\left(\mu_a + \mu_s'\right)\right]^{1/2} = \left(\mu_a / D\right)^{1/2}. \quad \text{(B.15)}$$

Solving the diffusion equation in the steady-state case yields a transmitted intensity for an infinite slab of scattering material:

$$I(\rho,d) = \frac{1}{2\pi}\sum_{k=0}^{\infty}\left[\frac{z_{-k}}{r_{-k}{}^3}\left(1+\mu_{eff} r_{-k}\right)\exp\left(-\mu_{eff} r_{-k}\right)\right.$$
$$\left. - \frac{z_{+k}}{r_{+k}{}^3}\left(1+\mu_{eff} r_{+k}\right)\exp\left(-\mu_{eff} r_{+k}\right)\right]. \quad \text{(B.16)}$$

REFERENCES

1 J. F. Kasting and J. L. Siefert, *Life and the evolution of Earth's atmosphere*, Science **296**, 1066 (2002).

2 T. R. Karl and K. E. Trenberth, *Modern global climate change*, Science **302**, 1719 (2003).

3 H. Akimoto, *Global air quality and pollution*, Science **302**, 1716 (2003).

4 P. Brimblecombe, Notes Rec. R. Soc. **32**, 123 (1978).

5 J. Gebhart, D. J. Rader, T. J. O'Hern, P. A. Baron, M. K. Mazumder, and Y. S. Cheng, in K. Willeke, P. A. Baron (Eds.), *Aerosol Measurement*, Chapters 15-17 (Van Nostrand Reinhold, New York 1993).

6 V. Ramanathan, P. J. Crutzen, J. T. Kiehl, and D. Rosenfeld, *Aerosols, climate, and the hydrological cycle*, Science **294**, 2119 (2001).

7 L. Morawska, N. D. Bofinger, and M. Maroni (Eds.), *Indoor Air* (Elsevier Science, Oxford 1995).

8 P. Weibring, H. Edner, S. Svanberg, G. Cecchi, L. Pantani, R. Ferrara, and T. Caltabiano, *Monitoring of volcanic sulphur dioxide emissions using differential absorption lidar (DIAL), differential optical absorption spectroscopy (DOAS), and correlation spectroscopy (COSPEC)*, Appl. Phys. B **67**, 419 (1998).

9 B. J. Finlayson-Pitts and J. N. Pitts Jr., *Tropospheric air pollution: ozone, airborne toxics, polycyclic aromatic hydrocarbons, and particles*, Science **276**, 1045 (1997).

10 T. E. Graedel, D. T. Hawkins, and L. D. Claxton, *Atmospheric Chemical Compounds: Sources, Occurrence, Bioassay* (Academic Press, Orlando 1986).

11 W. Michaelis, *Air Pollution* (Springer Verlag, Berlin, Heidelberg 1997).

12 R. W. Baubel, D. B Turner, and A. C. Stern, Fundamentals of Air Pollution (Academic Press, London 1994, 3rd edition).

13 R. P. Wayne, *Chemistry of Atmospheres* (Clarendon, Oxford 1985).

14 B. A. Trush, *The Chemistry of the Stratosphere*, Rep. Prog. Phys. **51**, 1341 (1988).

15 European Environment Agency, *Environment in the European Union at the turn of the century. Waste generation and management*, Report 2000; Chapter 3.7 (2000).

16 Air quality guidelines WHO; Chapter 2. *Air quality and health*. http://www.who.int/m/topics/air/en/index.html.

17 J. H. Seinfeld and S. N. Pandis, *Atmospheric Chemistry and Physics* (John Wiley & Sons, New York 1998).

18 E. G. Pacyna, J. M. Pacyna, and N. Pirrone, *European emissions of atmospheric mercury from anthropogenic sources in 1995*, Atmos. Environ. **35**, 2987 (2001).

19 S. H. Williston, J. Geophys. Res. **73**, 7051 (1961).

20 H. Edner, G. W. Faris, A. Sunesson, and S. Svanberg, Appl. Opt. **28**, 921 (1989).

21 UN-ECE, *Protocol on heavy metals. Convention long-range transboundary air pollution*, United Nations Economic Comission for Europe (1998).

22 EU Council Directive 1999/30/EC relating to limit values for sulphur dioxide, nitrogen dioxide and oxides of nitrogen, particulate matter and lead in ambient air (1999).

23 M. W. Sigrist (Ed.), *Air Monitoring by Spectroscopic Techniques* (John Wiley &Sons, New York 1994).

24 R. Stevens and J. Hodgeson, *Applications of chemiluminescent reactions to the measurement of air pollutants*, Anal. Chem. **45**, 443 (1973).

25 G. Wendel, D. Steadman, C. Cantrell, and L. Damrauer, *Luminol-based nitrogen dioxide detector*, Anal. Chem. **55**, 937 (1983).

26 C. Spiser, D. Kenny, G. Ward, I. Billick, and N. Leslie, *Evaluation of NO_2 measurement methods for indoor air quality applications*, J. Air Waste Management Assoc. **44**, 163 (1994).

27 Dobson, Harrison, (1926).

28 U. Platt, D. Perner, and H. W. Pätz, *Simultaneous measurement of atmospheric CH_2O, O_3, NO_2 by differential optical absorption*, J. Geophys. Res. **84**, 6329 (1979).

29 H. Edner, P. Ragnarsson, S. Spännare, and S. Svanberg, *Differential optical absorption spectroscopy (DOAS) system for urban atmospheric pollution monitoring*, Appl. Opt. **32**, 327 (1993).

30 P. Weibring, M. andersson, H. Edner, S. Svanberg, *Remote monitoring of industrial emissions by combination of lidar and plume velocity measurements*, Appl. Phys. B **66**, 383 (1998).

31 M. Sjöholm, P. Weibring, H. Edner, and S. Svanberg, *Atomic mercury flux monitoring using an optical parametric oscillator based lidar system*, Opt. Express **12**, 551 (2004).

32 E. D. Hinkley and P. L. Kelley, *Detection of air pollutants with tunable diode lasers*, Science **171**, 635 (1971).

33 J. Nordqvist and G. Somesfalean, *Perspectives on performance and policy in industry – environmental and quality concerns to enhance energy efficiency*, ECEEE 2003 Summer Study – Time to Turn Down Energy Demand, 783 (2003).

34 J. Nordqvist and G. Somesfalean, *Why industries environmental performance doesn't count*, China Environment Series **6**, 136 (2003).

35 S. Svanberg, *Laser spectroscopy in development*, Europhysics News **33**, 52 (2002).

36 R. N. Hall, G. E. Fenner, J. D. Kingsley, T. J. Soltys, and R. O. Carlson, *Coherent light emission from a GaAs junction*, Phys. Rev. Lett. **9**, 366 (1962).

37 M. I. Nathan, W. P. Dumke, G. Burns, F. H. Dill, Jr., and G. Lasher, *Stimulated emission of radiation from GaAs p-n junctions*, Appl. Phys. Lett. **1**, 62 (1962).

38 N. Holonyak, Jr. and S. F. Bevacqua, *Coherent (visible) light emission from* $Ga(As_{1-x}P_x)$ *junctions*, Appl. Phys. Lett. **1**, 82 (1962).

39 T. M. Quist, R. H. Rediker, R. J. Keyes, W. E. Krag, B. Lax, A. L. McWhorter, and H. J. Zeigler, *Semiconductor maser of GaAs*, Appl. Phys. Lett. **1**, 91 (1962).

40 I. Hayashi, M. B. Panish, P. W. Foy, and S. Sumski, *Junction lasers which operate continously at room temperature*, Appl. Phys. Lett. **17**, 109 (1970).

41 Zh. I. Alferov, V. M. Andreev, D. Z. Garbuzov, Yu. V. Zhilyaev, E. P. Morozov, E. L. Portnoi, and V. G. Trofim, *Investigations of the influence of the AlAs-GaAs heterostructure parameters on the laser threshold current and the realization of continuous emission at room temperature*, Sov. Phys. Semicond. **4**, 1573 (1971).

42 R. E. Slusher, *Laser technology*, Rev. of Mod. Phys. **71**, S471 (1999).

43 W. Chow, S. W. Koch, and M. Sargent III, *Semiconductor-Laser Physics* (Springer Verlag, Heidelberg 1994).

44 P. Agrawal and N. K. Dutta, *Semiconductor Lasers* (Van Nostrand Reinhold, New York 1993, 2nd edition).

45 K. Petermann, *Laser Diode Modulation and Noise* (Kluwer Academic Publishers, Dordrecht 1988).

46 C. Kittel, *Introduction to Solid State Physics* (Wiley & Sons, New York 1986, 6th edition).

47 J. Hecht, *The Laser Guidebook*, (McGraw-Hill, New York 1992, 2nd edition).

48 O. Svelto, *Principles of Lasers* (Plenum, New York 1989, 2nd edition).

49 J. C. Camparo, *The diode laser in atomic physics*, Contemp. Phys. **26**, 443 (1985).

50 A. A. Kosterev and F. K. Tittel, *Chemical sensors based on quantum cascade lasers*, IEEE J. Quantum Electron. **38**, 582 (2002).

51 F. Capasso, C. Gmachl, R. Paiella, A. Tredicucci, A. L. Hutchinson, D. L. Sivco, J. N. Baillargeon, A. Y. Cho, and H. C. Liu, *New frontiers in quantum cascade lasers and applications*, IEEE J. Sel. Topics Quant. Electron. **6**, 931 (2000).

52 C. Gmachl, A. Straub, R. Colombelli, F. Capasso, D. L. Sivco, A. M. Sergent, and A. Y. Cho, *Single-mode, tunable distributed-feedback and multiple-wavelength quantum cascade lasers*, IEEE J. Quantum Electron. **38**, 569 (2002).

53 S. Harris, *Redesigned VCSELs take a leap in power*, Opto & Laser Europe, April (2004).

54 S. Nakamura and G. Fasol, *The Blue Laser Diodes* (Springer Verlag, Heidelberg 1997).

55 http://www.nichia.co.jp

56 Y. R. Shen, *The Principles of Nonlinear Optics* (John Wiley & Sons, New York 1992).

57 R. W. Boyd, *Nonlinear Optics* (Academic Press, San Diego 1992).

58 M. M. Fejer, G. A. Magel, D. H. Jundt, and R. L. Byer, *Quasi-phase-matched second harmonic generation: tuning and tolerances*, IEEE. J. Quantum. Electron. **28**, 2631 (1992).

59 V. G. Dmitriev, G. G. Gurzadyan, and D. N. Nikogosyan, *Handbook of Nonlinear Optical Crystals* (Springer Verlag, Heidelberg 1991).

60 L. E. Myers, R. C. Eckhardt, M. M. Fejer, R. L. Byer, W. R. Rosenberg, and J. W. Pierce, *Quasi-phase-matched optical parametric oscillators in bulk periodically poled $LiNbO_3$*, J. Opt. Soc. Am. B **12**, 2102 (1995).

61 G. D. Boyd and D. A. Kleinman, *Parametric interaction of focused Gaussian light beams*, J. Appl. Phys. **39**, 3597 (1968).

62 T.-B. Chu and M. Broyer, *Intracavity cw difference frequency generation by mixing three photons and using Gaussian laser beams*, J. Physique **46**, 523 (1985).

63 D. Wandt, M. Laschek, K. Przyklenk, A. Tünnermann, and H. Welling, *External cavity laser diode with 40 nm continous tuning range around 825 nm*, Opt. Comm. **130**, 81 (1996).

64 F. Favre, D. Le Guen, J. C. Simon, and B Landousiers, *External-cavity semiconductor laser with a 15 nm continous tuning range*, Electron Lett. **22**, 795 (1986).

65 M. W. Fleming and A. Mooradian, *Spectral characteristics of external-cavity controlled semiconductor lasers*, IEEE J. Quantum. Electron. **QE-17**, 44 (1988).

66 L. Ricci, M. Weidemüller, T. Esslinger, A. Hemmerich, C. Zimmerman, V. Vuletic, W. König, and T. W. Hänsch, *A compact grating-stabilized diode laser system for atomic physics*, Opt. Comm. **117**, 541 (1995).

67 K. Liu and M. G. Littman, *Novel geometry for single-mode scanning tunable lasers*, Opt. Lett. **6**, 117 (1981).

68 R. P. Salathe, *Diode lasers coupled to external resonators*, Appl. Phys. **20**, 1 (1979).

69 G. Somesfalean, *Development and experimental evaluation of an optical sensor for aerosol particle characterization*, Lund Reports on Atomic Physics **LRAP-231** (1998).

70 S. Svanberg, *Atomic and Molecular Spectroscopy: Basic Aspects and Practical Applications* (Springer Verlag, Heidelberg 2004, 4th edition).

71 G. Somesfalean, J. Alnis, S. Svanberg, A. Derkatch, S. Mannervik, D. Rostohar, P. Royen, P. Schef, L.-O. Norlin, *Violet diode lasers in time-resolved stored-ion spectroscopy*, Physica Scripta **69**, 98 (2004).

72 E. Biémont, P. Palmeri, P. Quinet, G. Paquin, Z.G. Zhang, G. Somesfalean, S. Svanberg, *Measurement of radiative lifetimes and determination of transition probabilities of astrophysical interest in Ho III*, Monthly Notices of the Royal Astronomical Society **328**, 1085 (2001).

73 Z.G. Zhang, G. Somesfalean, S. Svanberg, P. Palmeri, P. Quinet, E. Biémont, *Radiative lifetime measurements and oscillator strengths of astrophysical interest in Ho III*, Astronomy & Astrophysics **384**, 364 (2002).

74 J. Humlicek, *Optimized computation of the Voigt and the complex probability function*, J. Quant. Spectrosc. Radiat. Transfer **27**, 437 (1982).

75 J. J. Olivieri and R. L. Longbothum, *Empirical fits to the Voigt line width: a brief review*, J. Quant. Spectrosc. Radiat. Transfer **17**, 233 (1977).

76 C. E. Wieman and L. Hollberg, *Using diode lasers for atomic physics*, Rev. Sci. Instrum. **62**, 1 (1991).

77 L. S. Rothman, C. P. Rinsland, A. Goldman, S. T. Massie, D. P. Edwards, J.-M. Flaud, A. Perrin, C. Camy-Peyret, V. Dana, J.-Y. Mandin, J. Schroeder, A. McCann, R. R. Gamache, R. B. Wattson, K. Yoshino, K. V. Chance, K. W. Jucks, L. R. Brown, V. Nemtchinov, and P. Varanasi, *The HITRAN molecular spectroscopic database and HAWKS (HITRAN Atmospheric Workstation): 1996 edition*, J. Quant. Spectrosc. Radiat. Transfer **60**, 665 (1998).

78 J. Orphal and K. Chance, *Ultraviolet and visible absorption cross-sections for HITRAN*, J. Quant. Spectrosc. Radiat. Transfer **82**, 491 (2003)

79 A. C. Vandaele, C. Hermans, P. C. Simon, M. Carleer, R. Colin, S. Fally, M. F. Mérienne, A. Jenouvrier, and B. Coquart, *Measurements of the NO_2 absorption cross-section from 42000 cm-1 to 10000 cm-1 (238-1000 nm) at 220 K and 294 K*, J. Q. S. R. T. **59**, 171 (1998).

80 N. Jacquinet-Husson, E. Arie, J. Ballard, A. Barbe, G. Bjoraker, B. Bonnet, L. R. Brown, C. Camy-Peyret, J. P. Champion, A. Chedin, A. Chursin, C. Clerbaux, G. Duxbury, J. M. Flaud, N. Fourrie, A. Fayt, G. Graner, R. Gamache, A. Goldman, V. Golovko, G. Guelachvili, J. M. Hartmann, J. C. Hilico, J. Hillman, G. Lefevre et al., *The 1997 spectroscopicGEISA databank*, IEEE J. Quant. Spectrosc. Radiat. Transfer **62**, 205-254 (1999).

81 http://ois.nist.gov/srmcatalog/datafiles

82 www.iupac-kinetic.ch.cam.ac.uk

83 http://nwir.pnl.gov

84 G. Hertzberg, Molecular Spectra and Molecular Structure. I-III (Van Nostrand, Princeton 1963, 1965, 1966).

85 J. C. Camparo, *The diode laser in atomic physics*, Contemp. Phys. **26**, 443 (1985).

86 P. Werle, *A review of recent advances in semiconductor laser based gas monitors*, Spectrochimica Acta, Part A **54**, 197 (1998).

87 A. Fried, B. Henry, and J. R. Drummond, *Tunable diode laser ratio measurements of atmospheric constituents by employing dual fitting analysis and jump scanning*, Appl. Opt. **32**, 821 (1993).

88 D. T. Cassidy and J. Reid, *High-sensitivity detection of trace gases using sweep integration and tunable diode lasers*, Appl. Opt. **21**, 2527 (1982).

89 C. Klimcak and J. Camparo, *Photothermal wavelength modulation of a diode laser*, J. Opt. Soc. Am. B **5**, 211 (1988).

90 G. D. Houser and E. Garmire, *Balanced detection technique to measure small changes in transmission*, Appl. Opt. **33**, 1059 (1994).

91 P. C. D. Hobbs, *Ultrasensitive laser measurements without tears*, Appl. Opt. **36**, 903 (1997).

92 E. I. Moses and C. L. Tang, *High sensitivity laser wavelength modulation spectroscopy*, Opt. Lett. **1**, 115 (1977).

93 G. C. Bjorklund, *Frequency-modulation spectroscopy: a new method for measuring weak absorptions and dispersions*, Opt. Lett. **5**, 15 (1980).

94 D. E. Cooper and T. F. Gallagher, *Double frequency modulation spectroscopy: high modulation frequency with low-bandwidth detectors*, Appl. Opt. **24**, 1327 (1985).

95 A. O'Keefe and D. A. G. Deacon, *Cavity ring-down optical spectrometer for absorption measurements using pulsed laser sources*, Rev. Sci. Instrum. **59**, 2544 (1988).

96 M. Nagele and M. W. Sigrist, *Mobile laser spectrometer with novel resonant multipass photoacoustic cell for trace-gas sensing*, Appl. Phys. B **70**, 895 (2000).

97 J. A. Silver and A. C. Stanton, *Optical interference fringe reduction in laser absorption measurements*, Appl. Opt. **27**, 1914 (1988).

98 H. Riris, C. B. Carlisle, R. E. Warren, and D. E. Cooper, *Signal-to-noise ratio enhancement in frequency-modulation spectrometers by digital signal processing*, Opt. Lett. **19**, 144 (1994).

99 J. Reid and D. Labrie, *Second-harmonic detection with tunable diode lasers - comparison of experiment and theory*, Appl. Phys. B **26**, 203 (1981).

100 W. Lenth, *High frequency heterodyne spectroscopy with current modulated diode lasers*, IEEE. J. Quantum Electron. **QE-20**, 1045 (1984).

101 J. M. Supplee, E. A. Whittaker, and W. Lenth, *Theoretical description of frequency modulation and wavelength modulation spectroscopy*, Appl. Opt. **33**, 6294 (1994).

102 D. E. Cooper and R. E. Warren, *Two-tone optical heterodyne spectroscopy with diode lasers: theory of line shapes and experimental results*, J. Opt. Soc. Am. B **4**, 470 (1987).

103 F. S. Pavone and M. Inguscio, *Frequency- and wavelength-modulation spectroscopies: comparison of experimental methods using an AlGaAs diode laser*, Appl. Phys. B **56**, 118 (1993).

104 L. Wang, H. Riris, C. B. Carlisle and T. F. Gallagher, *Comparison of approaches to modulation spectroscopy with GaAlAs semiconductor lasers: application to water vapor*, Appl. Opt. **27**, 2071 (1988).

105 G. Modugno, C. Corsi, M. Gabrysch, F. Marin, and M. Inguscio, *Fundamental noise sources in high-sensitivity two-tone frequency modulation spectrometer and detection of CO_2 at 1.6 μm and 2 μm*, Appl. Phys. B **67**, 289 (1998).

106 P. Werle, *Laser excess noise and inteferometric effects in frequency-modulated diode-laser spectrometers*, Appl. Phys. B. **60**, 449 (1995).

107 J. B. MacManus, P. L. Kebabian, and M. S. Zahniser, *Astigmatic mirror multipass cell for long-path-length spectroscopy*, Appl. Opt. **34**, 3336 (1995).

108 C. F. Bohren and D. R. Huffman, *Absorption and Scattering of Light by Small Particles* (John Wiley & Sons, New York, 1983).

109 H. C. van de Hulst, *Light Scattering by small Particles* (Wiley, New York 1957).

110 K. M. Case and P. F. Zweifel, *Linear Transport Theory* (Addison-Wesley Publishing Co., Reading, MA 1967).

111 U. Platt, Institute for Environmental Physics, University of Heidelberg, Heidelberg, Germany (personal communication, 2000).

112 S. Svanberg, M. Sjöholm, and G. Somesfalean, *Method and device for investigation of a surface layer*, Patent application PCT/SE03/00717 (2003).

113 T. V. Ward and H. H. Zwick, *Gas cell correlation spectrometer:GASPEC*, Appl. Opt. **14**, 2896 (1975).

114 K. F. Luft, *Über eine neue Methode der registrierenden Gasanalyse mit hilfe der Absorption ultraroter Strahlung ohne spectrale Zerlegung*, J. Tech. Phys. **24**, 97 (1943).

115 J. Sandsten, P. Weibring, H. Edner, and S. Svanberg, *Real-time gas-correlation imaging employing thermal background radiation*, Opt. Express **6**, 92 (2000).

116 J. Sandsten, H. Edner, and S. Svanberg, *Gas visualization of industrial hydrocarbon emissions*, Opt. Express **12**, 1443 (2004).